8-2006

The Effect of Star Formation on Observed Properties of High Redshift Absorption Systems

Yi-Jung Yang
University of Tennessee - Knoxville

To the Graduate Council:

I am submitting herewith a thesis written by Yi-Jung Yang entitled "The Effect of Star Formation on Observed Properties of High Redshift Absorption Systems." I have examined the final electronic copy of this thesis for form and content and recommend that it be accepted in partial fulfillment of the requirements for the degree of Master of Science, with a major in Physics.

Michael Guidry, Major Professor

We have read this thesis and recommend its acceptance:

Marianne Breinig, Chia C. Shih

Accepted for the Council:
Dixie L. Thompson

Vice Provost and Dean of the Graduate School

(Original signatures are on file with official student records.)

To the Graduate Council:

I am submitting herewith a thesis written by Yi-Jung Yang entitled “The Effect of Star Formation on Observed Properties of High Redshift Absorption Systems.” I have examined the final electronic copy of this thesis for form and content and recommend that it be accepted in partial fulfillment of the requirements for the degree of Master of Science, with a major in Physics.

Michael Guidry
Major Professor

We have read this thesis
and recommend its acceptance:

Marianne Breinig

Chia C. Shih

Accepted for the Council:

Anne Mayhew
Vice Chancellor and
Dean of Graduate Studies

(Original signatures are on file with official student records.)

The Effect of Star Formation on Observed Properties of High Redshift Absorption Systems

A

Thesis

Presented for the

Master of Science Degree

The University of Tennessee, Knoxville

Yi-Jung Yang

August 2006

Dedication

This thesis is dedicated to my family, especially to my mother, Hsiu-Yun Hsiao, who has always supported me, giving me endless love and encouragement.

Acknowledgements

I would like to thank my advisors Dr. Michael Guidry and Dr. Alexei Razoumov for their guidance, advice, support and limitless patience throughout the research. Also, I would like to thank the other members of my committee: Dr. Marianne Breinig and Dr. Chia C. Shih for their help and advice. Special thank to Dr. James E. Parks for his confidence on my teaching, and thanks to the Department for the award of a teaching assistantship to support my graduate studies.

Abstract

Damped Lyman-alpha absorber systems (DLAs) are thought to be one of the best probes to understand structure formation in the early universe. DLAs are defined as such systems with neutral hydrogen column density $N(HI) > 2\times10^{20}$ cm^{-2}. They have also been considered to be the most important neutral-gas reservoir for star formation at high redshift, and the key to uncovering the mystery of the progenitors of present-day galaxies. For many years, there has been a debate on the nature of the galaxies causing these absorptions at high redshift. One idea is that DLAs are small proto-galaxy clumps formed in the process of hierarchical structure formation. Another idea is that DLAs can be best explained with rapidly rotating, large, cold disks of galaxies. It is believed that through full understanding of the mechanism that control the processes, we are able to construct the history of galaxy evolution. In order to test on these ideas, we used high-resolution AMR (adaptive mesh refinement) hydrodynamics simulations to study kinematics properties and abundances of DLAs at redshift $z = 3$. Our simulations are based on standard cold dark matter cosmology (ΛCDM), and include full radiative transfer and star formation/feedback recipes, which are considered to be the two key ingredients to solve the low velocity-widths problem found in previous numerical simulations. Our results show that although we are able to reproduce the observed column density distribution, our velocity widths are still much lower than the observations. Further more, we plot line profiles through the points with highest radial velocities, which we believe are in the violent star or galaxy forming regions. From the single line profile, we can see some star formation/feedback effects by comparing the simulation runs with and without star formation/feedback. However, in a larger picture, these effects are not very obvious. This is probably due to the small volume size and insufficient grid-resolution. We conclude that it is essential to include full radiative transfer in order to reproduce reasonable HI column density distribution, and for further simulations, we should have larger volume size, and much higher resolution in order to resolve substructures such as star forming regions or supernova explosions.

Table of Contents

List of Figures

Chapter I

Introduction

Absorption lines in spectra of distant QSOs (quasi-stellar objects, or quasars) can be used as an efficient tool for probing structure formation in the early Universe. QSO absorbers are usually classified according to their neutral hydrogen column densities N(HI): Ly-alpha forest absorbers correspond to N(HI)< 10^{17} cm^{-2}, Lyman limit systems have 10^{17} < N(HI) < $2x10^{20}$ cm^{-2}, and damped Lyman-alpha (DLA) absorbers correspond to N(HI) > $2x10^{20}$ cm^{-2}. Most neutral hydrogen at high redshift is found in DLAs. On the other hand, the Ly-alpha forest contains highly ionized gas and is optically thin to Lyman limit (and higher energy) photons.

For many years, DLAs have been considered an important neutral gas reservoir for star formation at high redshifts. Stars are unlikely to form out of hot ionized gas; they tend to condense from cold neutral gas clouds. Therefore, it is necessary to have a large amount of neutral gas present in a star-forming region. DLAs are also thought to be likely candidates for high-redshift progenitors of present-day spiral disk galaxies. It is believed that through study of DLAs we'll be able to understand the early evolution of galaxies.

Formation of galaxies in the early Universe has been a subject of active debate, and several models have been proposed to explain the nature of DLAs. One school of thought is that DLAs are small proto-galactic clumps (i.e. dwarf galaxies) produced in the process of hierarchical structure formation in the Universe (with circular velocity $V_{circ} \leq$ 100 km/s). Another school of thought argues that DLAs can only be caused by large, rapidly rotating, cold galactic disks (with V_{circ} ~ 225 km/s). Prochaska & Wolfe (1997) investigated the metal-line kinematics and profile asymmetries of absorption lines, and made this latter conclusion. Hierarchical models of galaxy formation, on the other hand, predict that such massive disks are rare at z ~ 3. Prochaska & Wolfe also suggested two important tests that can be applied to most hierarchical structure formation models:

whether these models can reproduce the observed velocity width distribution, and whether they can account for the observed asymmetries in the absorption line profiles.

However, Haehnelt et al. (1998) showed that irregular proto-galactic clumps ($V_{circ} \leq 100$ km/s) could reproduce both the observed velocity width distribution and asymmetric profiles of the absorption lines. They then argued that the idea that DLAs at high redshift are related to large, rapidly rotating disks with $V_{circ} > 200$ km/s is not supported by observations. In their models, the required large velocity widths were produced as a result of rotation, random motions, infall, and merging. The asymmetries were mainly caused by random sampling of irregular density and velocity fields of individual halos, and by intrinsically asymmetric configurations arising when two or more clumps collide with each other. They found that the typical velocity dispersion of the dark matter halos required to give rise to the distribution of DLAs is about 100 km/s, and most of the standard hierarchical structure formation scenarios can easily reach the goal. Although the irregular proto-galactic clump models seem to fit observations well, there are still some reservations. Despite their high spatial resolution of 1 kpc and a mass resolution of $5x10^6$ M(solar), their simulation used a very small volume size (2 Mpc), and this may not truly represent typical DLAs in the cosmological context. High resolution is important for getting the rich substructure within the DLA region induced by the mergers of proto-galactic clumps in hierarchical structure formation scenarios. Furthermore, they did not include energy and momentum feedback due to star formation. Another important feature not included in their simulations is radiative transfer of the ultraviolet background (UVB). Instead of full transfer, they assumed a simple uniform radiation field with self-shielding above a critical density. This assumption directly affects the results of DLAs cross-sections, and therefore it is uncertain whether or not their numerical simulations are reliable.

In earlier studies based on hydrodynamic simulations in a cold dark matter (CDM) model with a range of column densities from 10^{14} cm^{-2} to 10^{22} cm^{-2}, Katz et al. (1996) and Hernquist et al. (1996) could reproduce the observed HI column density

distribution within a factor of a few. They used a more complex self-shielding correction showing that at low column densities < 10^{17} cm^{-2} the correction is rather small and the Ly-alpha forest naturally arises in the hierarchical structure formation of the CDM Universe. On the other hand, damped Lyman-alpha and Lyman limit systems, with HI column densities $\geq 10^{17} cm^{-2}$, are developed from radiatively cooled gas inside the dark matter halos, and the correction factor can be very large (up to a factor of 100). However, their calculations had very poor mass resolution of 10^{11} M(solar)/h.

Gardner et al. (1997, 2001) extended these earlier results by developing a new method to correct and to account for absorption in halos below the resolution limitations of the simulations. Their basic idea was to measure the relation between the DLA cross-section and the halo circular velocity in their hydrodynamic simulations and then convolve it with the Press & Schechter (1974) analytic halo mass function to obtain the cumulative abundance of DLAs in a large simulation volume. They were also able to reproduce the observed DLA abundance only if they required a cut-off circular velocity of haloes V_{circ} = 60 km/s. This is to say that under this cut-off value haloes do not host DLAs. This value of circular velocity corresponds to a mass M ~ 2×10^{10} M(solar)/h. The question is, in reality, whether halos with masses below 10^{10} M(solar)/h might still host a significant number of DLAs. Since their simulations could not resolve haloes with masses below this threshold, the abundance of DLAs could be either overestimated or underestimated. Therefore, simulations with high resolution are indeed needed for the further studies of DLA abundance.

Recent studies of Nagamine et al. (2004), however, did not use any correction for self-shielding. Instead, they use a new ‘conservative entropy’ formulation of smoothed particle hydrodynamics (SPH) developed by Springel & Hernquist (2002), which basically conserves entropy, momentum and energy. This treatment moderates the over-cooling problem seen in early SPH simulations. They also use a two-phase inter-stellar medium (ISM) model consisting of cold clouds with a hot ambient phase, with each gas particle representing a statistical mixture of cold and hot phases. In the ISM, cold clouds

grow through radiative cooling and that supplies baryons needed for star formation. When star formation occurs, supernova explosions then deposit energy back into the ISM and heat up the surrounding gas. As the cold gas is heated up, it then transitions back to its ambient phase. Galactic winds are also included into the models in order to study their effect on DLAs, galaxies, and the intergalactic medium (IGM). These outflows from high redshift galaxies play an important role in depositing metals into the IGM and affect the neutral gas distribution around the galaxies. Their results for the total HI mass density, the abundance of DLAs, and the column density distribution function agree well with observation at redshift z = 3. Similar to earlier studies by Katz et al. (1996), they conclude that DLAs arise naturally from radiatively cooled gas in dark matter haloes that form in the CDM Universe. However, they also indicated a significant drop-off in the DLAs abundance from redshift z = 3 to z = 1, and a weak evolution from z = 1 to z = 0. Their highest resolution simulation suggests that the cut-off halo mass for which DLAs do not exist is slightly above 10^8 M(solar)/h at z = 3 ~ 4, which is lower than previous estimates.

Although some of the simulations mentioned above agree well with observations, none of them have accounted for both kinematics and gas cross-section properties of DLAs in the same numerical model. Moreover, the earlier DLA simulations have only taken into account absorption by neutral gas in isolated galaxies. We should not exclude the possibility that a significant fraction of DLAs could be caused by neutral gas in tidal tails in galaxy mergers (Maller et al. 2001), or even in filaments where the gas is still falling into dark matter potential wells (Razoumov et al. 2005). Another problem of earlier simulations is that they do not include full radiative transfer. Although some of them apply a self-shielding correction method, it is still not clear how these self-shielding methods compare to models with full radiative transfer. It has been shown that radiative transfer effects could play an important role in cosmological simulations (Razoumov, 2005).

Razoumov et al. (2005) presented new high-resolution simulations of damped Lyman-alpha systems at redshift z = 3 using the adaptive mesh refinement (AMR) Eulerian hydrodynamic cosmological simulation code ENZO (Bryan & Norman 1999; O' Shea et al. 2004). These simulations included most of the key features required for modeling neutral gas in high column density absorber systems (i.e. dark matter dynamics, hydrodynamics, self-gravity, cooling and heating of gas, continuum radiative transfer of the UVB above the hydrogen Lyman limit, and gas chemistry.) They did not include star formation and feedback; instead their work focused on physical complications related to radiative transfer, as well as the effect of variations in the comoving volume size and numerical resolution. This study arrived at several important conclusions. First, it was found that models show a systematical trend in convergence towards the observed column density distribution with increasing grid resolution. Second, they found that not only the self-shielded halos can give rise to DLAs, but also tidal tails in mergers and various quasi-filamentary structures which often appear to be self-shielded against the UV background can produce DLAs. Third, they find that the mass cut-off threshold of halos for retaining neutral gas is ~ 7×10^7 M(solar)/h, which is lower than the previously reported estimates of M > 2×10^{10} M(solar)/h from Gardner et al. (1997, 2001), and M >10^8 M(solar)/h from Nagamine et al. (2004). Finally, they showed that models with full radiative transfer produce much higher DLA velocity widths than the commonly used self-shielding methods. On the other hand, their models produced much lower velocity widths compared to observations. Their velocity widths extend only to about 100 km/s, whereas the observed DLAs have a non-negligible population extending to 180-200 km/s.

This problem with low velocity widths can be also coupled to the infamous angular momentum problem in numerical galaxy formation (detailed references can be found in Sommer-Larsen, 2003), which is one of the unsolved problems in modern astrophysics. In the widely accepted hierarchical universe model, galactic disks form in the potential wells of dark matter halos as baryons cool and collapse into structures. Fall & Efstathiou (1980) showed that only when the collapsing gas retains most of its original angular momentum, can galactic disks match the inferred amount of angular momentum

to account for their observed spatial extent. However, most of the numerical simulations in CDM cosmology with the collapse scenario indicate that, when simulations only include radiative cooling, the infalling gas loses too much of its angular momentum, producing disks which are too small compared to observations. This is known as the angular momentum (AM) problem of disk galaxy formation. One reason for this problem is that, at early time, gas cooling occurs rapidly due to the larger gas densities, and the rate of inverse Compton cooling is large at high redshift. This leads to a rapid condensation of small, dense gas clouds, and before they ever get to merge to form disks they lose their energy and angular momentum to the surrounding dark matter halo. In order to prevent the collapse of small, dense clouds, and for them to preserve a large fraction of their angular momentum, we need new a mechanism. Weil, Eke & Efstathiou (1998) suggest that if early radiative cooling is suppressed, the numerical simulations can yield more "reasonably sized" disks. However, the physical mechanism of suppressing radiative cooling is unclear. Another solution was suggested by Sommer-Larsen & Dolgov (2001), by changing from the current CDM cosmology scenario to the warm dark matter (WDM) scenario. What is the best physical mechanism for suppressing early cooling? Can WDM cosmology solve the problems we encounter in CDM cosmology? Although these two questions remain unanswered, they give us a direction to think for the next step.

Another notable result from Prochaska & Wolfe, 2001 is that after comparing their observations of the kinematic characteristics of DLAs with results from earlier numerical SPH simulations (Haehnelt 1998, Gardner 2001), they found that simulations failed to match the observed properties of DLAs. In their discussion, they highlight two competing constraints on galaxy formation scenarios from observations. First, in order to match the observed number of DLAs, the mass spectrum must include enough low-mass halos. On the other hand, the number of low mass halos that can contribute to DLAs is limited by the velocity-width distribution. Although earlier SPH simulations show good agreement with either of these two constraints, the simulations cannot satisfy both constraints simultaneously. Prochaska & Wolfe point out possible problems with these

simulations: incorrect determination of the cross sectional dependence of dark matter halos which contain DLAs, or the faulty determination of circular velocity limits and velocity widths. They suggest several possible solutions to the problem: (1) introduce other substructure physics to eliminate neutral gas from within the low mass halos, (2) include star formation and star formation feedback, and finally (3) run the simulations with a larger cosmological volume (> 20 Mpc/h) and higher resolution to resolve more substructures with DLAs in detail.

My research is an extension of the work done by Razoumov et al. (2005), except that we use a newer version of the AMR code ENZO, which includes the effect of star formation (implemented in the new "star maker" and "star feedback" routines) to investigate whether star formation and feedback can affect the column density distribution and the velocity widths. However, at the current stage, we can achieve only a relatively low base grid resolution of 64^3 with 7 levels of refinement by a factor of two in the co-moving box size = 4 Mpc/h (This is due to shortage of time, and unavailability of supercomputing resources). In Razoumov et al. (2005) the maximum grid resolution was 128^3 with a maximum of seven levels of refinement and a co-moving box size of 8 Mpc/h. In the near future, we should be able to use the same grid resolution, and our final goal is to achieve a grid resolution of 256^3, with at least 7 levels of refinement, in combination with a larger volume size -- this of course all depends on availability of computing resources. All our simulations were run with standard flat, cold dark matter cosmology (ΛCDM), assuming a total matter density (baryons + DM) $\Omega_m = 0.3$, a dark energy density $\Omega_\Lambda = 0.7$, a baryon density $\Omega_b = 0.045$, and a Hubble constant $h = 0.67$.

The goal of this thesis is to study whether star formation can solve the low velocity-width problem. This thesis is organized as follows: In chapter II, I review QSO absorption line systems with examples and explain their properties in more detail. In chapter III, I review some of the basic physics for star formation, star formation feedback, and show the examples how star formation affects our simulations. In chapter IV, I review the methodology behind radiative transfer and related issues in cosmological

simulations, such as local vs. background heating. In chapter V, I give some background information on the numerical AMR simulation code ENZO we used, and the initial conditions setup. And finally, in the last chapter, I show our simulation results, analysis, compare them with current observations and draw conclusions.

Chapter II

QSO Absorber Systems

Quasars are very luminous point-like sources, probably the brightest optical sources in the known universe, and have very high redshifts indicating that they are very distant from Earth. Quasars also emit very strong electromagnetic radiation at various wavelengths. That is why they are considered to be the best source of light with which we can probe the physical properties of the universe in absorption, such as the cosmic chemical abundances, and history of star formation. It is believed that quasars are powered by accretion on supermassive black holes. After these black holes stop significant accretion, quasars become normal galaxies.

2.1 Types of Line Systems

There are several types of QSO absorption line systems: Lyman alpha forest, Lyman limit, and damped Lyman-alpha systems. In the later section, I will discuss properties and characteristics of these absorption line systems. However, in our research, we focus on searching for DLA lines. I will discuss more in detail why we look for DLA lines and why these lines are important. I will also give more examples to show DLA properties.

2.1.1 Lyman-alpha forest

Lyman-alpha forest lines are numerous weak lines from very low-density hydrogen clouds, which are partially or fully ionized. The “forest” is due to the fact that photons, which come from the distant quasar, show the Hubble redshift that depends on the distance between the observer and the quasar. The Lyman-alpha forest absorbers are selected for HI column densities smaller than 10^{17} cm^{-2}.

2.1.2 Lyman limit systems (LLS)

LLs are very rare and exhibit strong hydrogen absorption line regions with relatively high column density between $10^{17}cm^{-2}$ and $2x10^{20}$ $cm^{-2.}$

2.1.3 Damped Lyman-alpha absorption (DLA) systems

Similar to LLs, DLAs are very rare and strong hydrogen absorption line regions with column densities greater than $2x10^{20}$ cm^{-2}. DLAs are very interesting systems as they have very strong and wide damping wings in the observed absorption line profiles. DLAs are thought to be progenitors of disk galaxies.

In order for stars to form in the interstellar gas clouds, it is crucial to have neutral gas since stars would not form out of ionized gas. What makes DLAs unique from other absorbers is that they contain most of the neutral hydrogen gas while the other type of absorbers contain mostly ionized gas. This leads us to believe that since DLAs dominate the neutral gas content of the universe, they are an important neutral gas source for star formation at high redshifts.

From Figure 2.1, we can see continuous spectrum of a distant quasar, showing different absorption lines. On the right side of the spectrum, around the wavelength 285 nm, we can see the Lyman-alpha emission line. Towards the left from Lyman-alpha emission is the Lyman-alpha forest, with a series of weak absorption lines. Next to the Ly-alpha forest, around 260 nm, there are a few Lyman-limit lines. And finally at wavelength 225 nm, we see this strong, deep, damped Lyman-alpha line. Because all these absorbing clouds have smaller redshifts than the quasar, they are closer to us. As a result, their absorption lines are all on the bluer, or the shorter wavelength side of the quasar emission line.

Similar to Figure 2.1, Figure 2.2 is another quasar spectrum from the Keck Telescope. We can see a series of Lyman-alpha absorption lines. Near the center, we also see a very clear, strong DLA. The second part of this figure shows the metal absorption lines from heavy elements, such as C, Si, Mg, Al and Fe…etc. They are mostly from merging galaxies. These metal absorptions lines trace the chemical content history of these cloud systems through various chemical abundances.

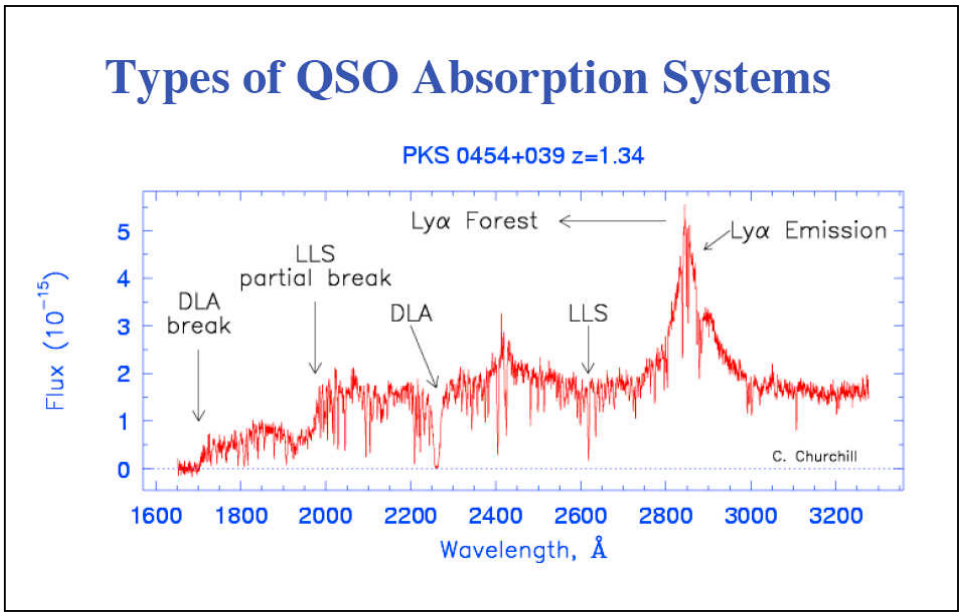

Figure 2.1 Types of QSO absorption systems at redshift z = 1.34.

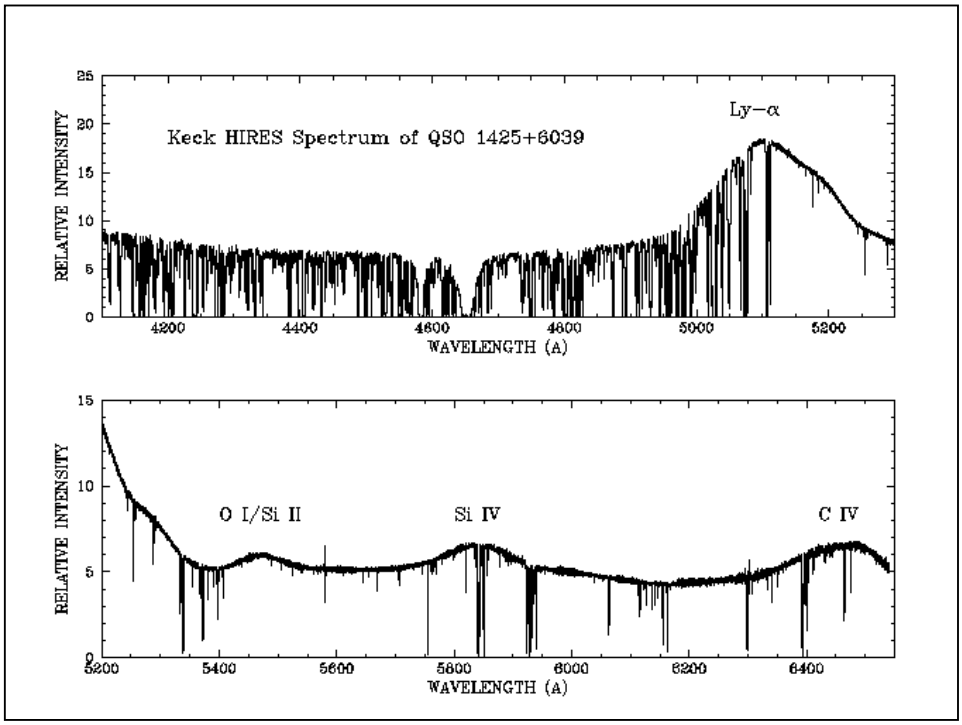

Figure 2.2 Keck HIRES spectrum of QSO 1425+6039

2.2 Distribution of Column Densities

At high redshifts, we can distinguish neutral gas from ionized gas by looking at the HI column density. If the HI column density is less than $2x10^{20}$ cm^{-2}, the gas is more likely to be ionized. If the HI column density is greater than $2x10^{20}$ cm^{-2}, the gas is more likely to be neutral. The $2x10^{20}$ cm^{-2} threshold is indeed significant.

Figure 2.3 shows the distribution of these three neutral hydrogen column densities. Note that the Ly-alpha forest is optically thin to Lyman limit systems (and higher energy) photons. In our research, we only focus on searching for DLA systems. Therefore we set the threshold $2x10^{20}$ cm^{-2} in our simulation code to find DLA abundance.

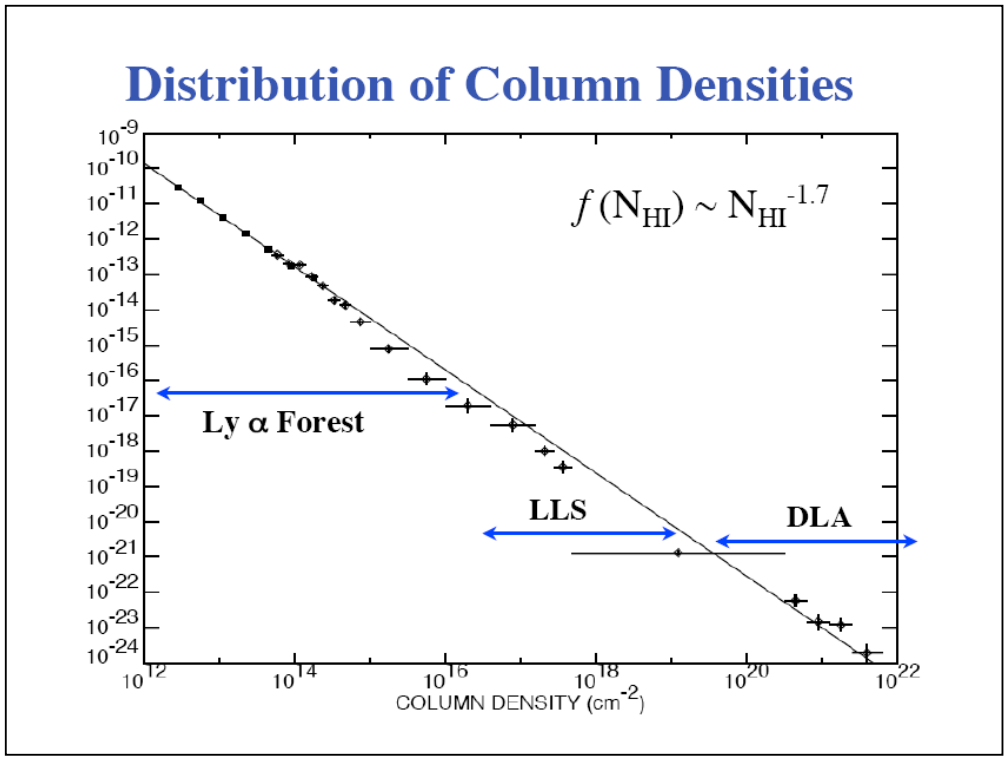

Figure 2.3 Distribution of HI column densities. (Hu et al. 1995)

The observational data were taken from the SDSS (Sloan Digital Sky Survey). Figure 2.4 shows an estimate of the column density distribution f(N, X) from a sample of over 600 damped Lyman-alpha systems. The figure also shows the three possible best-fit functions to describe f(N, X). Below are the formulations of these three best-fit functions:

1. Single power-law function: $f(N,X) = k_1 N^{\alpha 1}$
2. Γ Function: $f(N,X) = k_2 (N/N_\gamma)^{\alpha 2} \exp(-N/N_\gamma)$
3. Double power-law function: $f(N,X) = k_3 (N/N_\gamma)^{\beta}$

where $\beta = \alpha_3$ when $N < N_d$ and $\beta = \alpha_4$ when $N \geq N_d$

We will compare our computational results to the SDSS DLA data fit with the Γ function with z = 2.5 to 3.0, and z = 3.0 to 3.5.

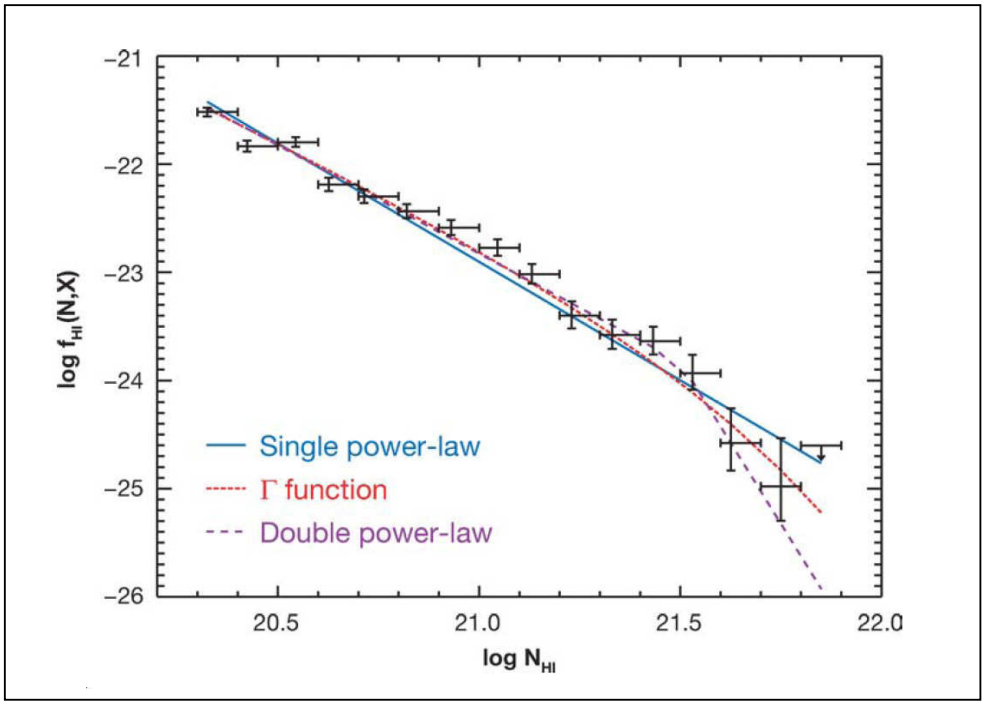

Figure 2.4 The HI frequency distribution $f_{HI}(N,X)$ for all of the damped Ly-alpha systems identified in the SDSS-DR3_4 sample (at redshift z = 3.06).

2.3 Formalism

To derive an expression for the column density distribution, we first define the number of absorbers per line of sight with HI column densities in the interval (N, N+dN) and redshifts in the interval (z, z+dz) as

$$dN(N,z) = n_{comoving}(N,z)A(N,z)(1+z)^3 \left| c\,dt/dz \right| dNdz ,$$

where $n_{comoving}(N,z)dN$ = the comoving density of absorbers in the interval (N, N+dN) at redshift z, and A(N,z) = the absorption cross-section at (N, z). We define

$$dX \equiv (H_0/c)(1+z)^3 \left| c\,dt/dz \right| dz .$$

If we write $\frac{dN(X)}{dX} = \int_{N_{\min}}^{N_{\max}} dNf(X,N)$, we then have

$$f(N,X) \equiv (c/H_0)n_{comoving}(N,X)A(N,X) .$$

Chapter III

Star Formation

Star formation often leads to very energetic astrophysical processes (i.e. supernova explosions, stellar winds, UV radiation) that can ionize or expel neutral gas, preventing it from future condensation.

3.1 Star Formation Rate Evolution

Many theoretical and observational studies show that the cosmic star formation rate rises towards high redshift, even beyond z = 3. (Nagamine et al. 2004) This means that conversion of gas into stars occurs more rapidly in these high redshift galaxies. It is thought that star formation has a very strong link to the evolution of clusters of galaxies through metal enrichment of the intergalactic medium. Since DLAs dominate the neutral hydrogen content of the universe at redshift z = 3, they are considered to be an important reservoir of HI gas for star formation at high redshift. This is the reason why we study the abundance of DLAs using a series of cosmological AMR simulations while varying star formation and the feedback strength at redshift z = 3.

Figure 3.1 shows the star formation rate evolution vs. redshift and time. We can see that the star formation rate reaches its maximum at around redshift z = 3. Although the star formation rate beyond z = 3 is still not clear, the occurrence of numerous star forming activities at redshift z = 3 is certain.

3.2 Star Formation in Simulation Codes

Here I describe the numerical method we use to create star particles in our code. We create stars according to the following selection criteria:

(1) check to see if it is the finest level of adaptive mesh refinement,

(2) check to see if the density is greater than the critical density,

(3) check to see if the flow is convergent in the cell,

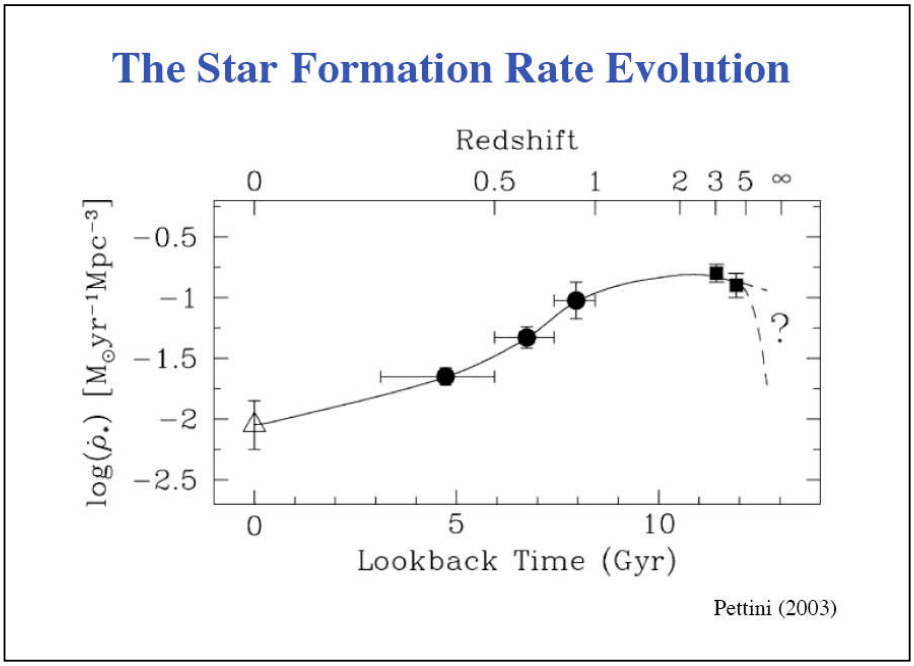

Figure 3.1 The star formation rate evolution.

(4) check to see if the cooling time is less than the dynamical time

$$t_{dyn} = \sqrt{\frac{3\pi}{32Gd_{tot}}}\ ,$$

$$d_{tot} = d + d_m\ ,$$

here d is the density,
d_m is the dark matter density,
and t_{dyn} is dynamical time

(5) check to see if the gas mass is greater than the Jeans mass

If all conditions above are met, and the gas mass in the cell is greater than the threshold, then a star particle is created. The program then sets the particle metal fraction, and removes the mass from the grid. If not, the program will go to the next cell and will repeat the same process. Figure 3.2 is a flow chart of the star formation process in the code.

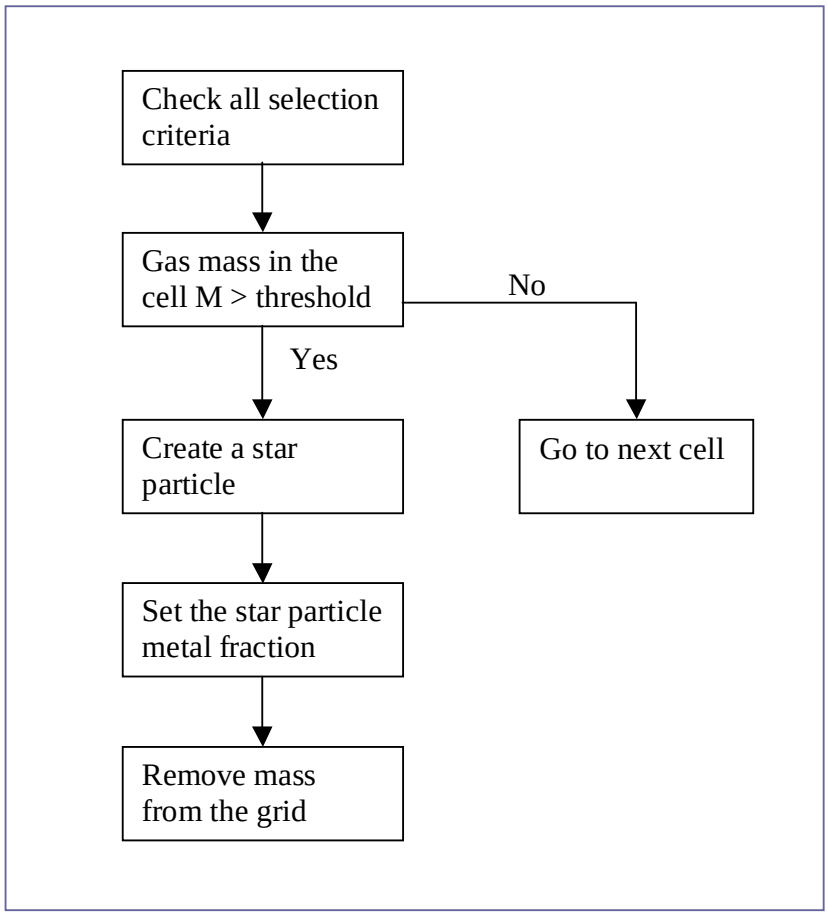

Figure 3.2 Star formation processes.

3.3 Star Formation Feedback

If star particles are created over a long period of time, the program assumes that these particles would actually lose their mass over time exponentially due to feedback (i.e. winds, supernovae).

We first determine how much gas would turn into star particles during the time-step.

$$x_{v1} = \frac{t - t_{cp}}{t_{dp}}$$

$$x_{v2} = \frac{t + dt - t_{cp}}{t_{dp}}$$

t = current time
t_{cp} = creation time of particle
t_{dp} = dynamical time of zone in which particle created
dt = current time step

We then calculate the initial mass of the star particle:

$$m_{initial} = \frac{m_p}{\left\{1 - m_{eject}\left[1 - \left(1 + x_{v1}\right)e^{-x_{v1}}\right]\right\}},$$

where $m_{\_eject}$ = fraction of the stellar mass ejected back into the gas (wind, supernovae), and m_p = new particle mass.

Finally, we calculate the star particle mass formed in the time-step:

$$m_{form} = m_{initial}\left\{\left[\left(1 + x_{v1}\right)e^{-x_{v1}}\right] - \left[\left(1 + x_{v2}\right)e^{-x_{v2}}\right]\right\},$$

the remaining particle mass then becomes,

$$m_p = m_p - m_{form} m_{eject}\,.$$

Chapter IV

Radiative Transfer

Radiative transfer plays a very important role in many astrophysical processes such as cosmic reionization, regulation of star formation in high redshift systems, evaporation of planetary disks, and formation of planetary nebulae… In order to understand the early reheating and reionization of the intergalactic medium (IGM), as well as structure and evolution of high redshift absorption systems, many simulations have been performed. However, radiative transfer effects have either been ignored or treated as a simple self-shielding correction in most simulations.

Although many approximations have been developed, such as space-averaged fields, self-shielding corrections, and the diffusion approximation, these approximations do not account for full multi-dimensional radiative transfer and therefore cannot provide accurate results, especially when compared to observations.

Modeling radiative transfer and feedback in cosmological hydrodynamical simulations with good accuracy is crucial, and it proved to be extremely challenging in the present work. In the following sections, I will introduce some basic formulations of radiative transfer, describe how radiative transfer is implemented in the numerical simulations, and finally I will compare the simulation results with and without radiative transfer.

4.1 Radiative Transfer Formulation

The classical transfer equation was proposed by Kirchhoff (1860)

$$\frac{1}{c}\frac{\partial I_\nu}{\partial t} + \hat{n}\cdot\nabla I_\nu = \varepsilon_\nu - \kappa_\nu I_\nu \qquad (1)$$

where, $I_\nu \equiv I(t, \vec{x}, \hat{n}, \nu)$ is the intensity of the radiation field, $\hat{n}$ is a unit vector along the direction of ray propagating through space, ε_ν is the emission coefficient, and κ_ν is the absorption coefficient.

To adapt it to cosmological problems, Abel & Norman (1998) rewrote this classical radiative transfer equation in the new form:

$$\frac{1}{c}\frac{\partial I_\nu}{\partial t} + \frac{\hat{n}\cdot\nabla I_\nu}{\bar{a}} - \frac{H(t)}{c}\left(\nu\frac{\partial I_\nu}{\partial \nu} - 3I_\nu\right) = \varepsilon_\nu - \kappa_\nu I_\nu \qquad (2)$$

where $H(t) \equiv \frac{\dot{a}}{a}$ is the time-dependent Hubble constant, and

$\bar{a} = \frac{1+z_{emission}}{1+z}$ is the ratio of cosmic scale factors between photon emission at frequency ν and the present time t.

There are two modifications in this equation compared to the classical radiative transfer equation. First of all, $\bar{a}$ in the second term accounts for the path-length change along the ray due to the expansion of the universe. Secondly, the additional third term represents cosmological redshift and dilution. Including this equation into cosmological simulations proved to be very challenging, especially considering the high dimensionality and high angular resolution needed in such simulations. Therefore, it is necessary to develop some approximations to accomplish the task.

Comparing the second and third terms of the modified equation, we find that on small scales the Hubble flow is negligible and we can satisfy the condition $\left|\nu\frac{\partial I_\nu}{\partial \nu}\right| \le I_\nu$ for continuum radiation. Furthermore, for constant absorption and emission, the time derivative term can also be dropped for simplicity. Therefore, all that is left is a static transfer equation:

$$\hat{n}\cdot\nabla I_\nu = \varepsilon_\nu - \kappa_\nu I_\nu . \qquad (3)$$

However, this equation needs to be used with caution. At small distances from the point source, this simplified case would break down, since the ionization front would expand faster than the speed of light. To avoid this problem, one does not evolve ionization fronts very close to sources.

Let us decompose the radiation field into a point source component and a diffuse component:

$$I_\nu \equiv I_\nu^{src} + I_\nu^{diff} \ , \qquad (4)$$

where I_ν^{src} is highly anisotropic, and I_ν^{diff} is nearly isotropic.

Using the linearity of the radiation field, we can write the transfer equation for the diffuse component as

$$\hat{n} \cdot \nabla I_\nu^{diff} = \kappa_\nu (S_\nu - I_\nu^{diff}) \, , \qquad (5)$$

$$\hat{n} \cdot \nabla I_\nu^{src} = -\kappa_\nu I_\nu^{src} \, . \qquad (6)$$

For point sources, all photons stream radially and we can compute transfer as simple attenuation along the radius. Here $S_\nu \equiv \frac{\varepsilon_\nu}{\kappa_\nu}$ is the source function. For $\kappa_\nu(x) = const$, equation (6) can then be solved with a simple analytic solution:

$$I_\nu(x_1) = I_\nu(x_0) e^{-\tau} = I_\nu(x_0) e^{-\kappa_\nu (x_1 - x_0)} \, . \qquad (7)$$

4.2 Radiative Transfer in Simulation Code

Figure 4.1 is an example of a flow chart for a given computational cell in simulations (Mellema et al., 2005).

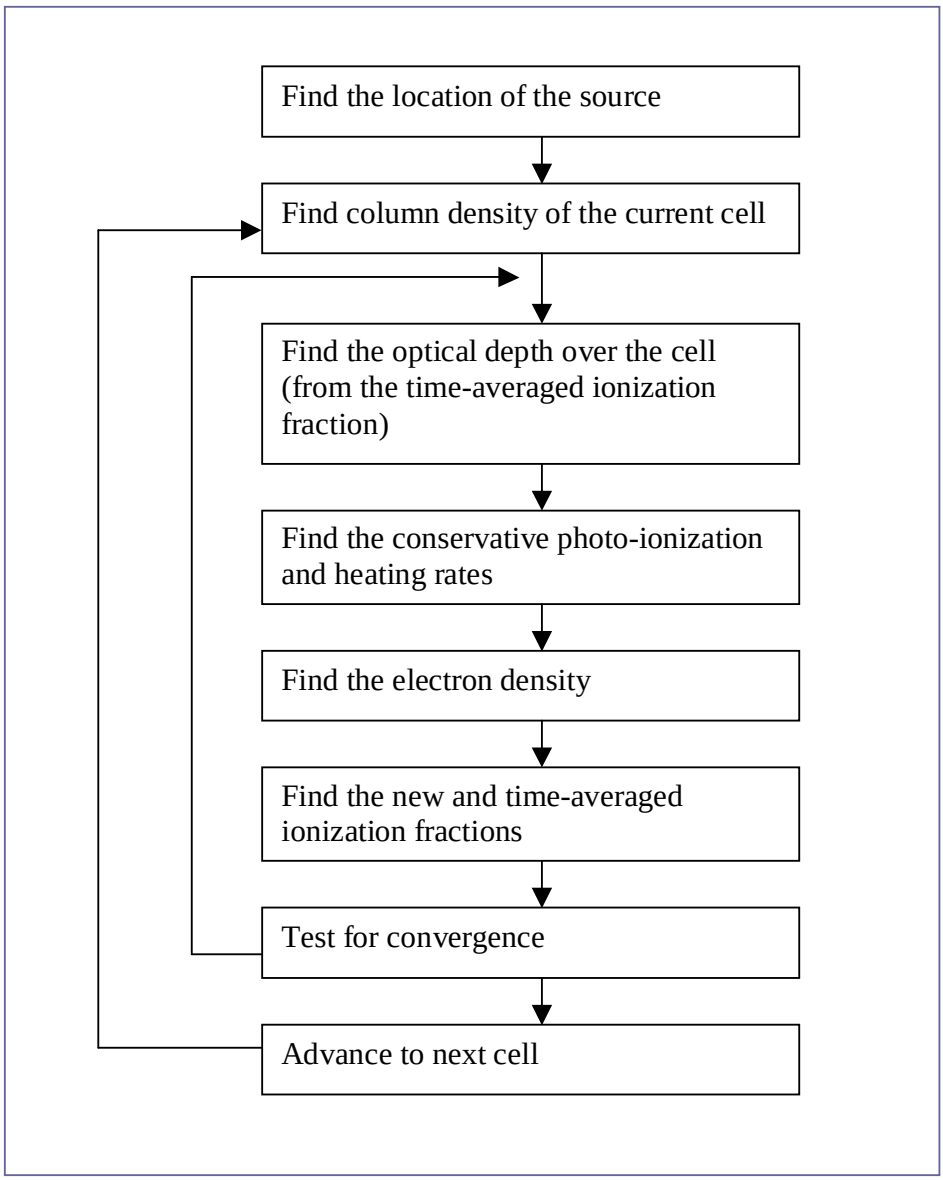

Figure 4.1 Flow chart of radiative transfer.

Our simulations involve two steps associated with cooling and heating. In the first step, the Enzo simulations solve the local heating (low angular resolution) with hydrodynamic equations simultaneously. Several models for uniform ultraviolet background radiation have been implemented, and they do a good job coupling with hydrodynamics. The disadvantage of radiative transfer in Enzo is that we can only assume the UVB from the local environment and must ignore the sources from outside of the volume. Therefore, in the second step, we take the output from Enzo and post-process it with another radiative transfer code at higher angular resolution. This radiative transfer code assumes that the UVB sources are outside the volume. The code uses the updated radiation field to compute the ionization structure and temperature and then iterates until the equilibrium position of HI, HeI and HeII ionization fronts are found. In order for the UVB to reach convergence, at least 10~20 iterations are needed.

Figure 4.2 shows the convergence of the UVB through iterations. The UVB converges quickly and reaches a plateau at around iteration 20, and after that remains rather constant.

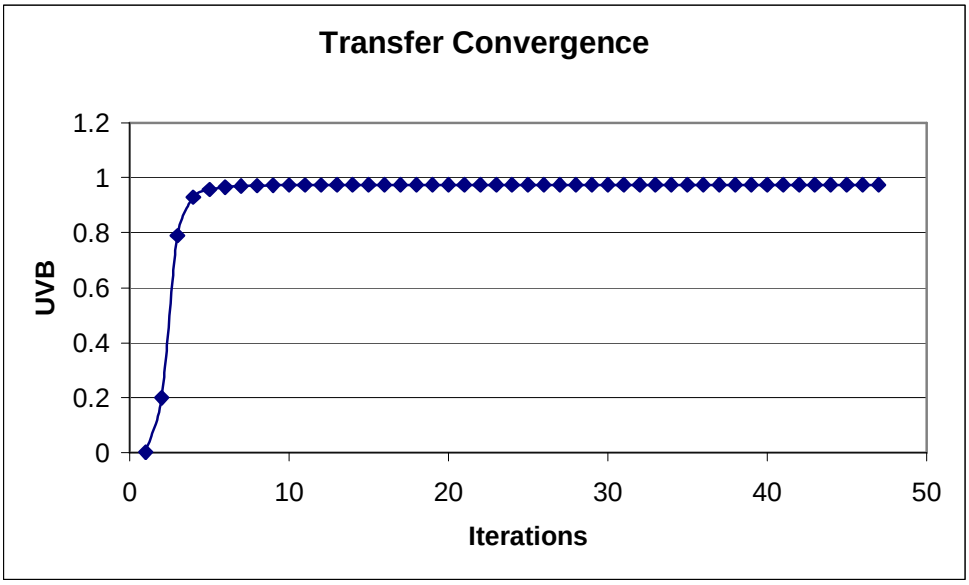

Figure 4.2 Radiative transfer convergence.

4.3 Comparison of Column Density Map with and without Radiative Transfer

In our simulations, in addition to varying the star formation/feedback efficiency, we also compare the same models with and without full radiative transfer. The results show that, without full radiate transfer, we obtain much lower HI column densities and smaller velocity widths. With full radiative transfer, we can reproduce the observed column density distribution and obtain more realistic velocity widths compared to the ones without transfer. Figure 4.3 shows the projected neutral hydrogen column density map without running through full radiative transfer, and figure 4.4 is the same model but with full radiative transfer. The color scale on the right shows the column densities. The DLA range is around the color light green and light blue. Comparing these two figures we can see the latter one (with radiative transfer) contains more DLAs than the one without radiative transfer.

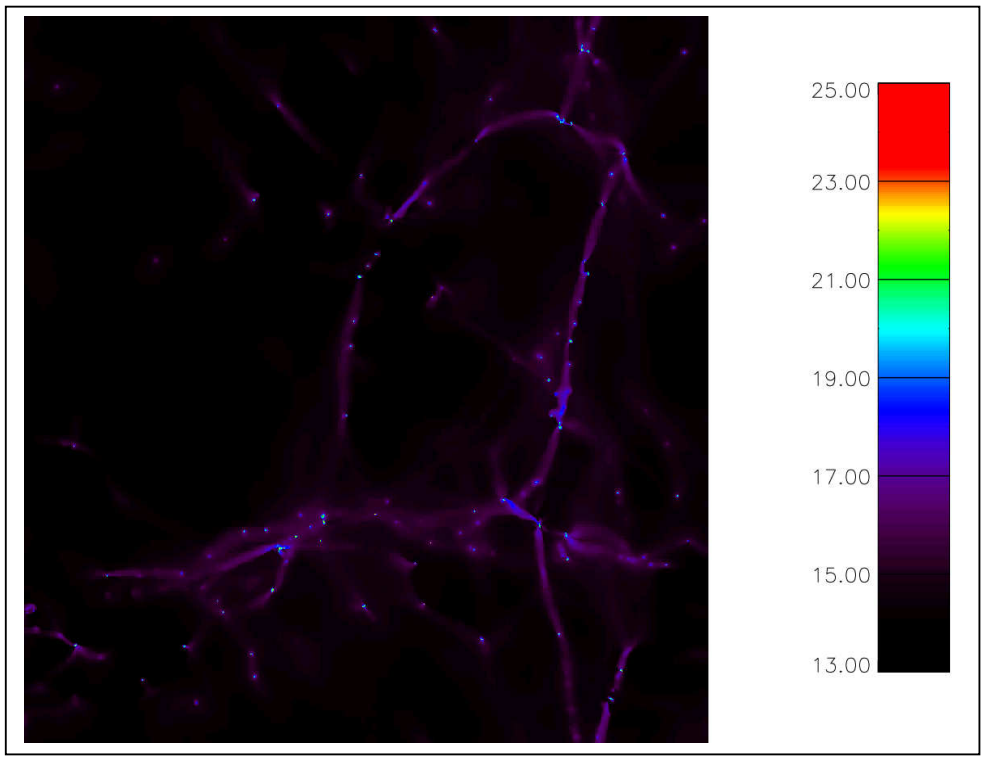

Figure 4.3 Projected column density map without full radiative transfer.

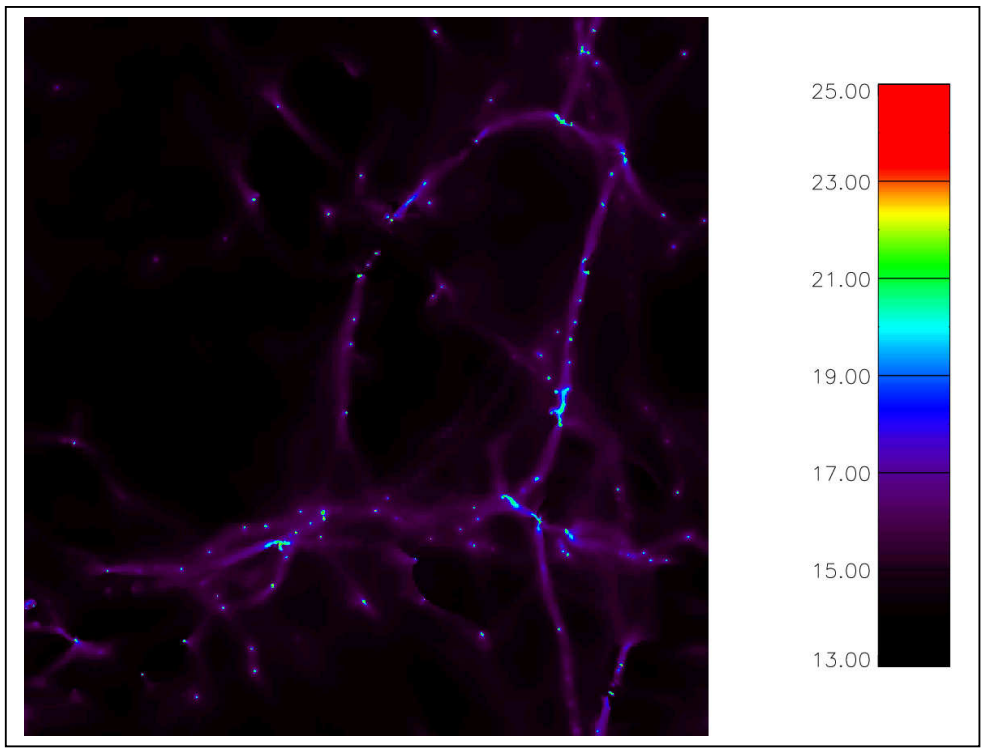

Figure 4.4 Projected column density map with full radiative transfer.

Chapter V

Numerical Simulation

5.1 AMR-Enzo

Enzo is an MPI-parallel three-dimensional Eulerian hydrodynamics block-structured adaptive mesh refinement (AMR) cosmology code. This code is written in a mixture of C, C++, and Fortran languages, with higher level functions and data structures implemented in C++, while computationally intensive lower level functions are implemented in Fortran. In addition to modeling cosmological structure formation, Enzo can also be used to simulate a wide rage of astrophysical phenomena (O'Shea et al. 2004).

Enzo, in principal, would distribute the workload within each level of the AMR hierarchy across all processors. By definition, a grid is a "real" grid on a particular processor if its data is allocated to that specific processor, and is a "ghost" grid if its data is allocated on a different processor. Each grid is a real grid on one specific processor, and a ghost grid on all others. When exchange of information is needed, MPI is then used to transfer the mesh or particle data between processors.

Figure 5.1 shows a two-dimensional AMR hierarchy. The left side of the figure shows six total grids distributed across two processors in a three level hierarchy. And the right side of the figure shows a grid zones map where a block of real zones is surrounded by layer of ghost zones. Real zones are used to store the data field parameters, and ghost zones are used to store values from their neighboring grids, parent grids or the external boundary conditions.

5.2 Physics in Enzo

Enzo solves dark matter N-body dynamics by using the particle-mesh technique, and hydrodynamics by a modified version of the piecewise parabolic method (PPM) of

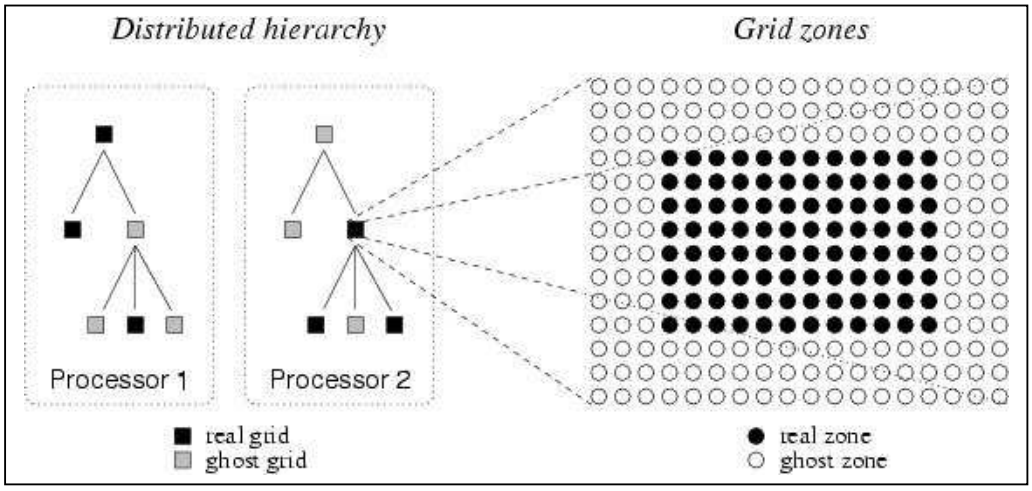

Figure 5.1 Left side is a picture of real and ghost grids in a hierarchy, and the right side is a picture of real and ghost zones in a grid (O'Shea et al. 2004).

Woodward & Colella. In addition to these main functions, several new physics features have been implemented in the Enzo code, such as radiative cooling and heating, different models for uniform ultraviolet background (UVB) radiation, and star formation/feedback.

5.2.1 Dark matter Dynamics

Approximately 85% of the matter in the universe is dark matter; therefore when simulating large-scale cosmological structures we need to solve the dark matter dynamics. Enzo uses the particle-mesh N-body method to calculate collision-less particle dynamics. The particle trajectories are governed by the set of coupled equations shown below, but the cosmology terms are omitted for simplicity (O'Shea et al. 2004).

$$\frac{d\vec{x}_p}{dt} = \vec{v}_p \ ,$$

$$\frac{d\vec{v}_p}{dt} = -\nabla\phi \ ,$$

where $\vec{x}_p$ and $\vec{v}_p$ are the position and velocity vectors of particle and $-\nabla\phi$ is the gravitational force term. The solution to the above equations can be found by solving Poisson's equation

$$\nabla^2\phi = 4\pi G\rho \ ,$$

where ρ is the density of baryon gas (collisional) and particles (collision-less).

5.2.2 Hydrodynamics

PPM has been modified in order to solve the cosmological problems. For example, the conservation laws of fluid mass, momentum and energy density are implemented in the comoving coordinates and are modified to include gravity.

5.2.3 Cooling & Heating

The cooling and ionization of gas is very important in astrophysical processes. Therefore, two radiative cooling and several uniform UVB models have been implemented. The first radiative cooling model assumes that all chemical species in the baryonic gas are in equilibrium and the cooling rates can be calculated directly from a cooling curve assuming metallicity $Z = 0.3Z_0$. The second model solves a reaction network of 28 equations that includes collisional and radiative processes for 9 species (H, H^+, He, He^+, He^{++}, H^-, H_2^+, H_2 and e^-).

The present-day universe is full of low-density gas, which has been ionized by ultraviolet background radiation from quasars, stars and other sources. We can study the properties of these ionized gases through Lyman-alpha forest absorptions systems. This then can be used to determine several important cosmological parameters, and to understand the formation and evolution of structures in the universe. As the UVB plays a very important role in determining the ionization of the gases, it is crucial that we model the effects of UVB as accurate as possible. Several models for assuming a uniform UVB radiation have been implemented and used in Enzo code.

5.2.4 Star Formation/ Feedback

One of the most important astrophysical processes, which affects the formation, and evolution of galaxies, is star formation and its feedback. The star formation and feedback recipe in Enzo converts gas particles into star particles, and then these particles evolve and eject their thermal energy and metals back into the gas via galactic winds.

5.3 Simulations

5.3.1 Initial Conditions

All our simulations were run with standard flat cold dark matter cosmology ΛCDM, assuming a total matter density (baryons + DM) $\Omega_m = 0.3$, a dark energy density $\Omega_\Lambda = 0.7$, a baryon density $\Omega_b = 0.045$, and a Hubble constant $h = 0.67$.

In total, we ran 7 models-- modnosf, mod0, mod1, mod2, mod3, efficient2, and extreme case-- increasing the amount of stellar energy deposited as: (1) thermal energy back into the gas, radiated in (2) stellar UV photons and in (3) quasar UV photons.

The run modnosf has no star formation and feedback at all, and efficient2 has exactly the same setup as mod2 but with a lower star maker density threshold and a shorter dynamical time allowing for an "easier' conversion of gas into stars.

We evolve the models from redshift z = 99 to z = 3. We set the maximum level of refinement to 7. Below I show a basic simulations setup:

Grid dimensions = 64×64×64 (N_{base})
Volume Size = 4 Mpc/h (L_{box})

To calculate mass resolution, we use:

$$\Delta M \approx 3.2\times10^{6}\left(\frac{L_{box}}{Mpc}\right)^{3}\left(\frac{N_{base}}{32}\right)^{-3} M_{\odot}$$

So our mass resolution is,

$$\Delta M \approx 3.2\times10^{6}\left(4\right)^{3}\left(\frac{64}{32}\right)^{-3} \approx 2.56\times10^{7} M_{\odot}$$

Table 5.1 is a list of simulation models with various input strength for star formation and star feedback strength. Also note that modnosf has no star particle creation and feedback, and efficient2 has a lower star maker density threshold and a shorter dynamical time. Extreme is the case with relatively much higher feedback comparing to other models.

Table 5.1 List of models with various star formation and star feedback strength.

	Star Energy to Thermal Feedback	**Star Energy to Stellar UV**	**Star Energy to Quasar UV**
modnosf	0	0	0
mod0	1.e-7	3.e-8	5.e-8
mod1	1.e-6	3.e-7	5.e-7
mod2	1.e-5	3.e-6	5.e-6
mod3	1.e-4	3.e-5	5.e-5
efficient2	1.e-5	3.e-6	5.e-6
extreme	high	high	high

5.3.2 Example of Strong Star Formation and Feedback

Figure 5.2 shows an example of strong star formation effects on these simulations (extreme). Note that this model is not a realistic case. The real situation probably falls between mod1 and mod2. Here I just want to show how star formation would effect simulations with the increasing strength of feedback. With stronger thermal feedback, we can see some evidence of violent astrophysical processes, such as the shock wave and the stellar winds created by supernova explosions. In this figure, we can see more structures compared to other models.

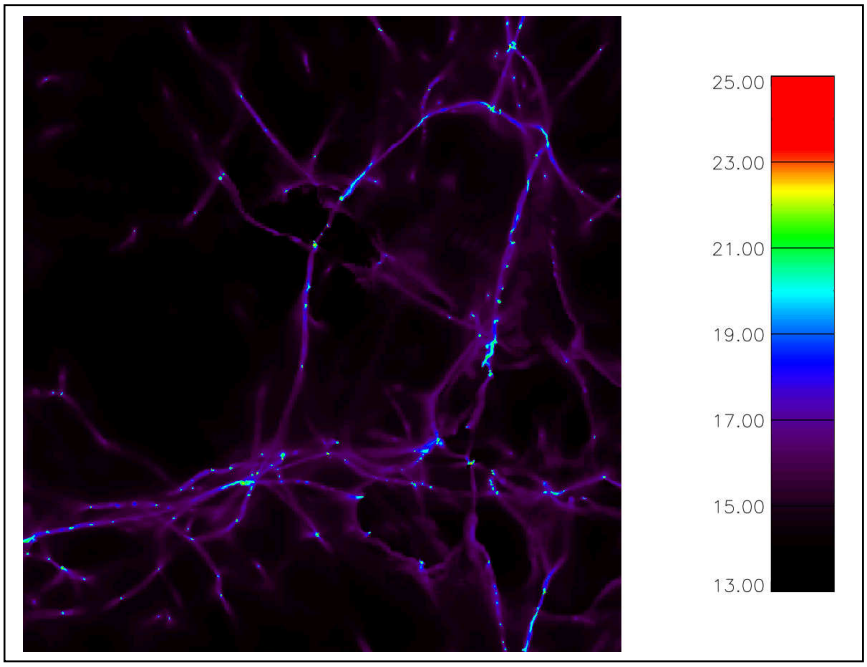

Figure 5.2 Projected column density map of model with extreme star formation and feedback.

Chapter VI

Results

6.1 Column Density Distribution

We first compare our results with and without transfer. Figure 6.1 is the column density frequency distribution for runs modnosf, mod0, mod1, mod2 and mod3 (solid lines from finest to thickest) without radiative transfer. Figure 6.2 is the column density frequency distribution for the same runs as in figure 6.1 (lines from finest to thickest as well) but with full radiative transfer. The dashed and dotted lines in both figures are the Γ-function fits to the SDSS DLA survey data from Prochaska et al. (2005) for z = 2.5-3.0(dashed) and z = 3 – 3.5 (dotted). We can see in the figure 6.1 that at lower column densities all the lines are much lower than the observations, indicating that the runs without transfer do not reproduce the observed DLA abundance. However, lines in Figure 6.2 are very close to the observations. It is therefore important to run full radiative transfer for all the simulations in order to reach the required DLA abundance, instead of the simple approximation of the uniform UVB.

One question is whether running full radiative transfer will really yield the correct DLA abundance, or does it over-estimate it? Enzo code assumes a uniform UV background in all cells, even within dense clouds, when dealing with cooling and heating problems. On the contrary, the radiative transfer code assumes that the sources of UVB are outside the volume, and it computes self-shielding for dense regions where more hydrogen remains neutral. However, our current implementation of radiative transfer does not include photons produced locally inside the star formation regions. We suspect that the real picture is probably in between these two models. The best approach is to combine the two methods, however it has proved to be a very difficult task to accomplish with current limited computational power.

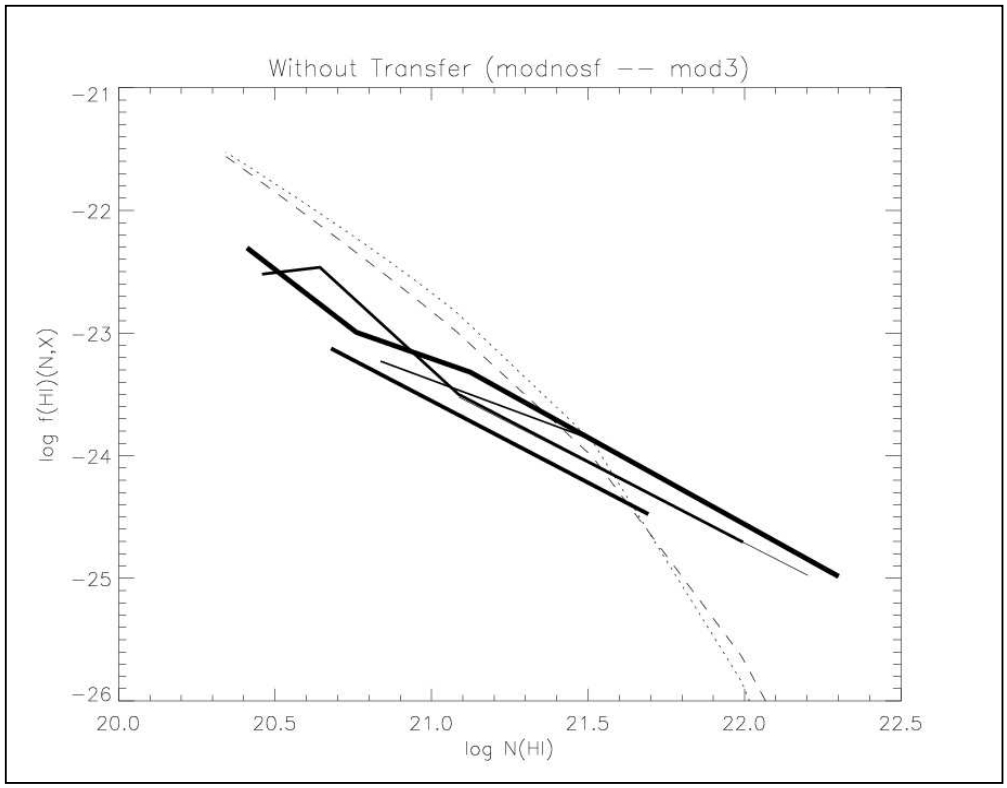

Figure 6.1 Column density frequency distribution for simulation models modnosf to mod3, without radiative transfer.

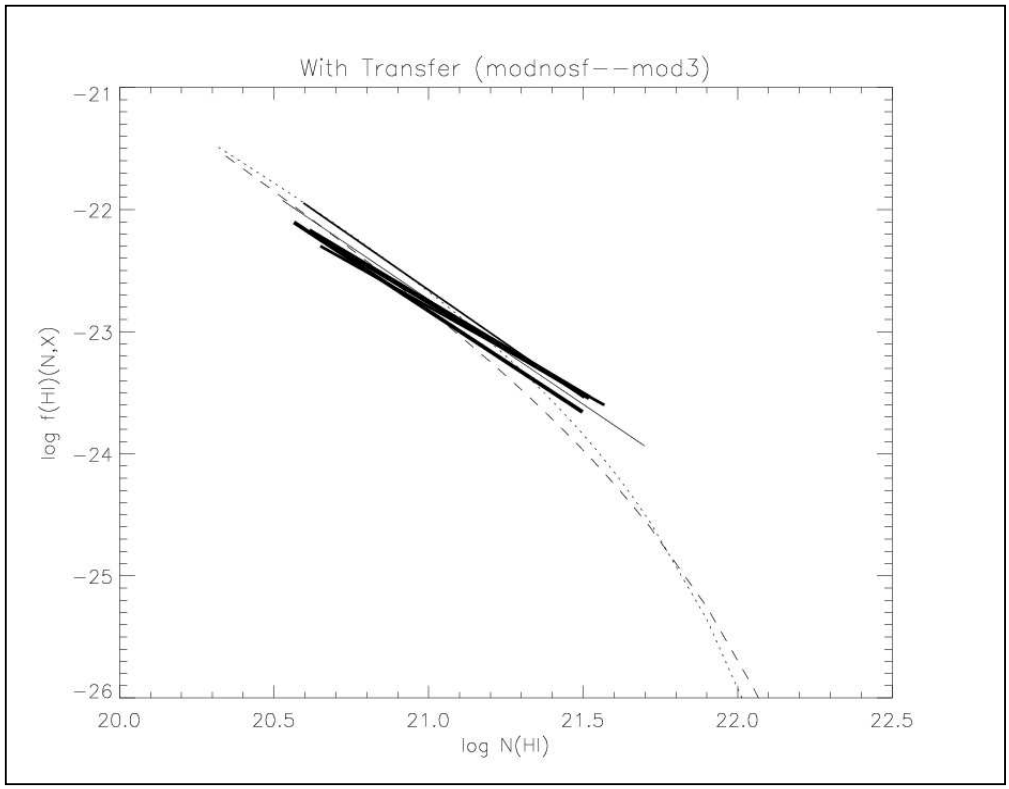

Figure 6.2 Column Density frequency distribution for simulation models modnosf to mod3, with radiative transfer.

6.2 DLA Line Density vs. Velocity Widths

Figure 6.3 shows the DLA line density vs. velocity width plot for runs modnosf, mod0, mod1, mod2, and mod3 (solid lines from finest to thickest respectively) without radiative transfer. Figure 6.4 is DLA line density vs. velocity width plot for the same runs with full radiative transfer. The dotted line is the observation. Comparing Figures 6.3 and 6.4, we find that runs with transfer produce higher velocity widths than runs without transfer.

However, although we can reproduce the observed column density distribution (from Figure 6.2), our velocity widths are still much lower than those from observations. Apparently, star formation does not produce the desired effect so far. This might be due to the low grid resolution. With only 64^3 base grid resolution, it is difficult to resolve substructures such as star forming regions or supernova shells. Therefore it is essential to go up to even higher grid resolution and further investigate the effect of star formation.

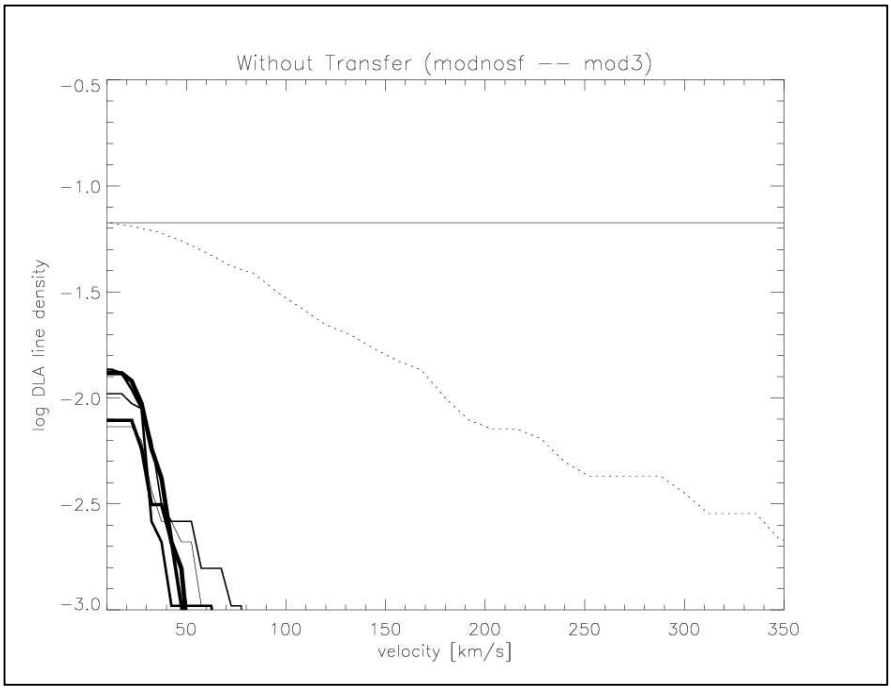

Figure 6.3 DLA line density vs. velocity (km/s) for simulation models modnosf to mod3, without radiative transfer.

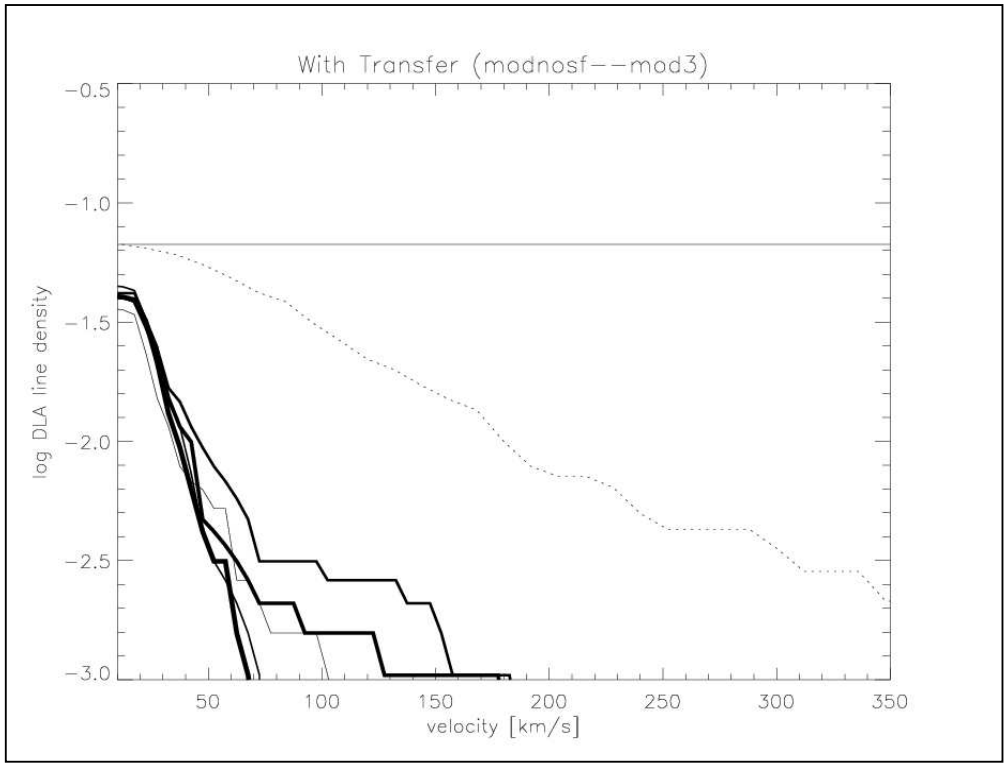

Figure 6.4 DLA line density vs. velocity (km/s) for simulation models modnosf to mod3, with radiative transfer.

6.3 Comparison of Column Density Maps in High Radial Velocity Region

In this section, I select one fixed region with relatively high radial velocities in all models (modnosf, mod0—mod3 and efficient2), from Figure 6.5 to 6.11, and show their projected neutral hydrogen column density maps. We can see as star formation and the thermal feedback strength increase, there are more violent activities (gas turbulence) in the volume. These might be due to shock waves from supernova explosions and stellar winds. Note that mod3 has the highest star formation feedback strength, but it does not show too much activity. We suspect that this is because the thermal feedback is too strong. It eventually wipes out all the gas around the first generation stars and ionizes the entire surrounding medium, leaving no chance for further condensations and star formation. (The color scale below is indication for neutral hydrogen density. DLAs fall between the light green and light blue region.)

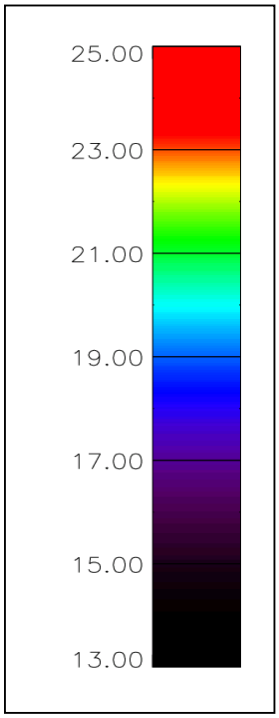

Figure 6.5 HI column density scale.

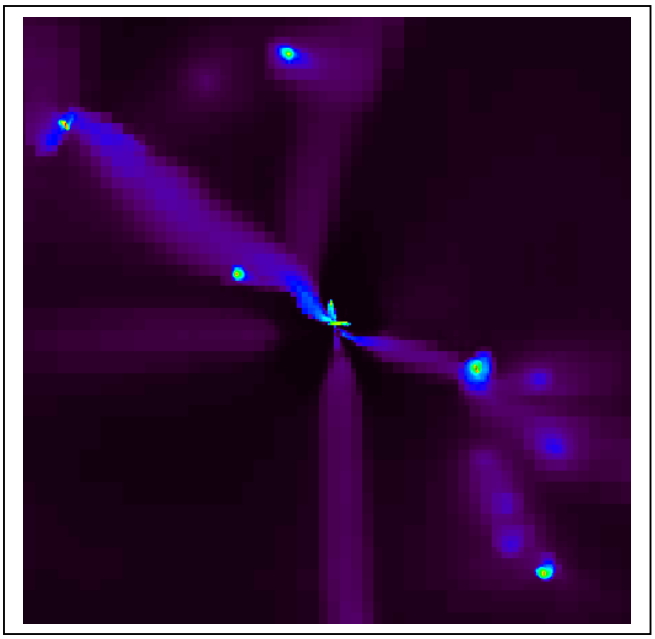

Figure 6.6 Selected high radial velocity region for modnosf.

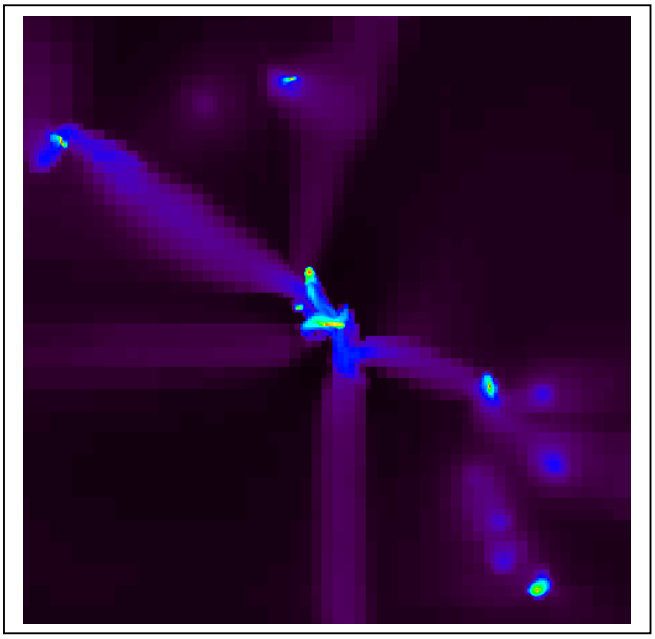

Figure 6.7 Selected high radial velocity region for mod0.

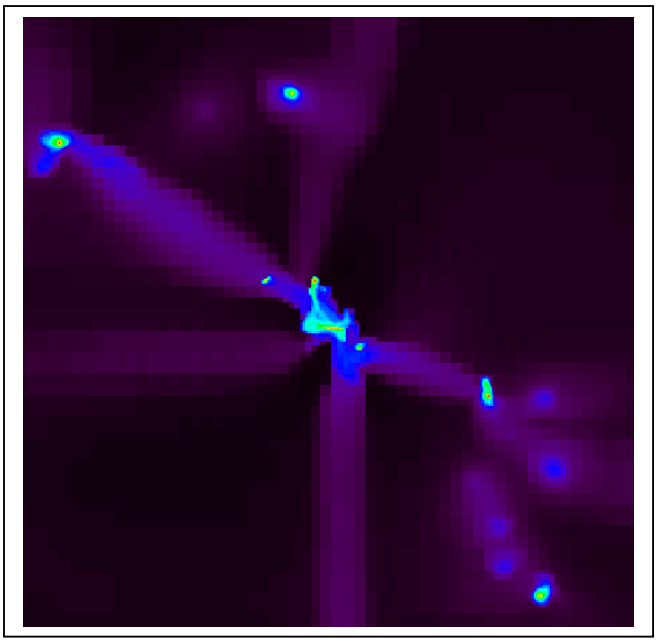

Figure 6.8 Selected high radial velocity region for mod1.

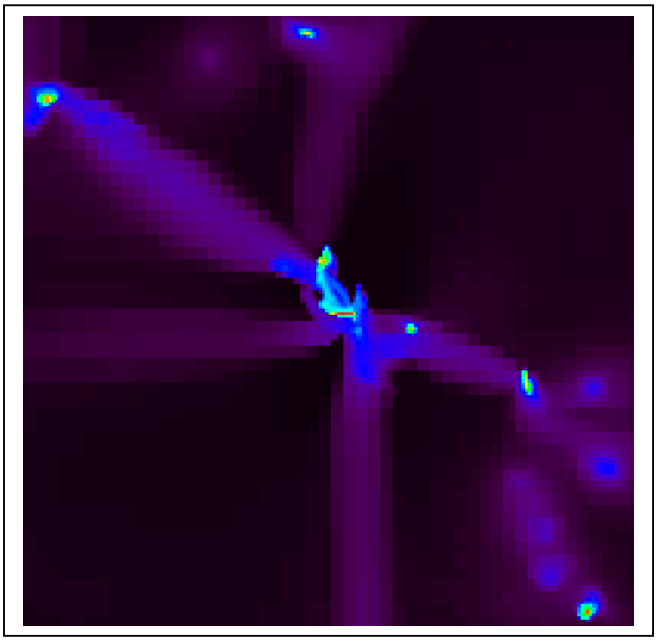

Figure 6.9 Selected high radial velocity region for mod2.

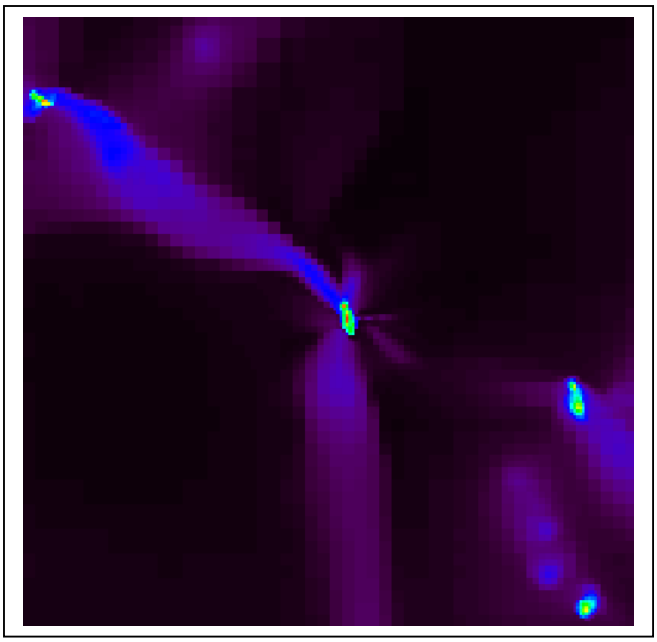

Figure 6.10 Selected high radial velocity region for mod3.

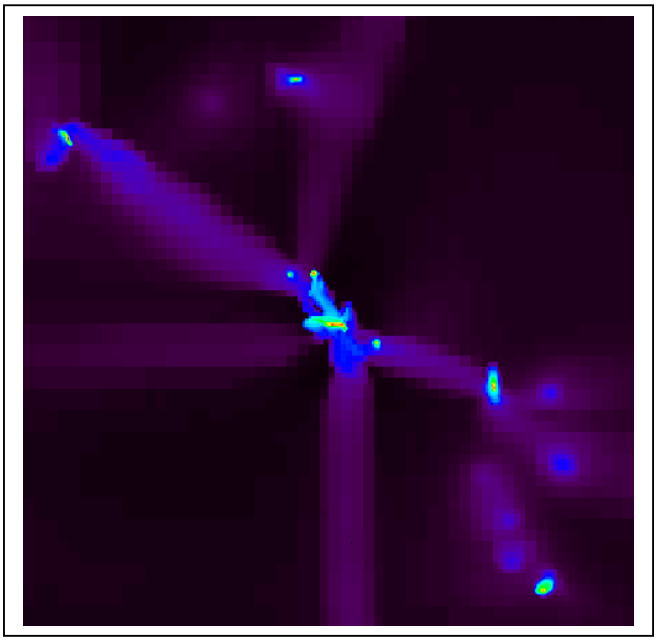

Figure 6.11 Selected high radial velocity region for efficient2.

Figures 6.12 and 6.13 are two other examples of selected high radial velocity column density maps for runs modnosf and mod3. In the mod3 run, a galaxy forming on the lower-left has some very interesting features. We can actually see some spiral arms produced (indicating that the velocity dispersion in that specific region must be very high) and a smaller galaxy merging with the larger galaxy. Comparing models with no star formation and with strong star formation/feedback, we can see that star formation and feedback produce effects, but they are generally complex. (From the velocity width plot, we did not see much effect.) In some cases, we see clear evidence that feedback plays an important role causing strong, violent activity, but not in other cases. In future work we will need to study the star formation effects in more detail and also reconstruct the star formation history as a function of redshift.

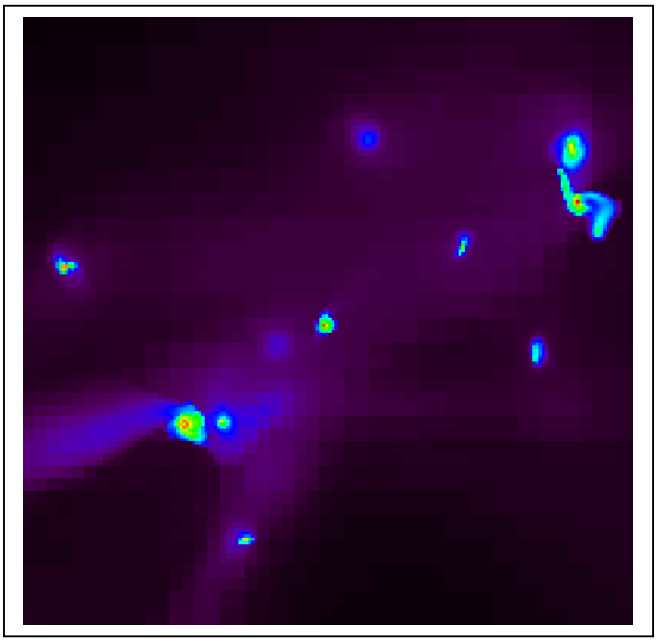

Figure 6.12 Another selected high radial velocity region for modnosf.

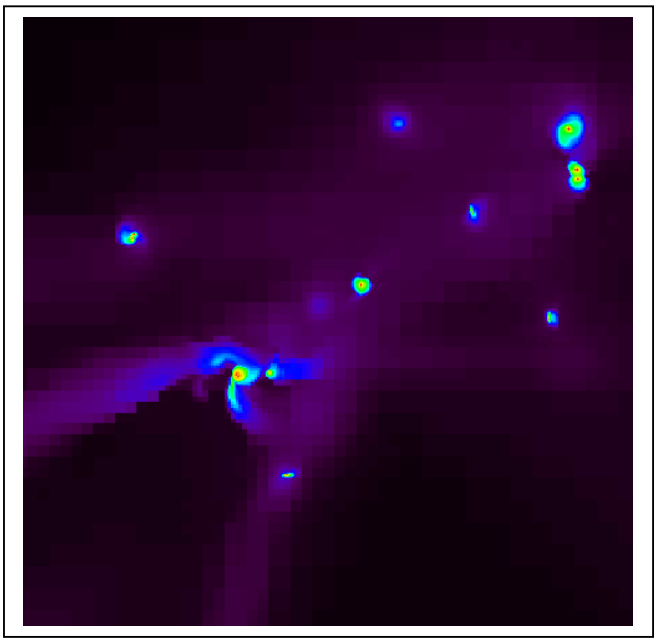

Figure 6.13 Another selected high radial velocity region for mod3.

6.4 Density and Velocity Profiles along a Line-of-Sight

Figures 6.14 to 6.19 show distribution of physical variables along two selected lines of sight for modnosf and mod2. Figures 6.14 and 6.15 show the total density rho vs. physical coordinate along the z direction. Figures 6.16 and 6.17 show the HI density vs. physical coordinate along z. And finally Figures 6.18 and 6.19 give the radial velocity vs. physical coordinate. Comparing the models with and without the star formation, we see some interesting differences. The features of mod2 look more complex, and it seems to have more substructures than in modnosf. For example, in Figure 6.14 we see that modnosf has only one sharp peak (center of galaxy) located around 900 kpc, along with a very small peak next to it. However in Figure 6.15 we see several peaks across from around 850 kpc to 950 kpc, indicating that there are probably more substructures created due to the star formations process (i.e. supernova explosions or stellar winds). We can see similar effects in Figure 6.16 and 6.17, and also Figure 6.18 and 6.19.

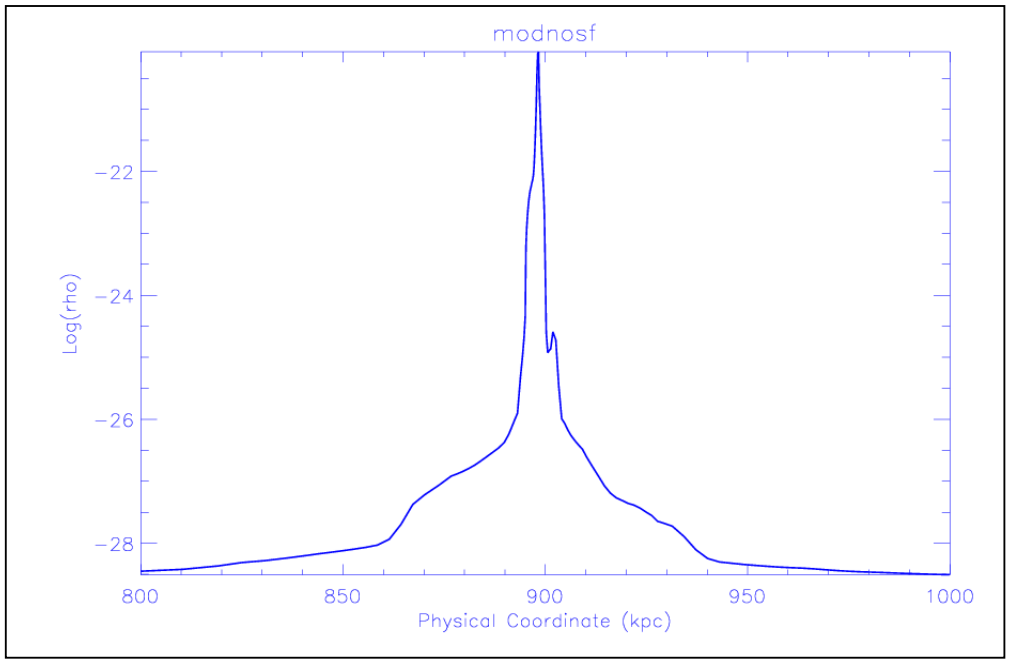

Figure 6.14 Total density (rho) vs. physical coordinate along z for modnosf.

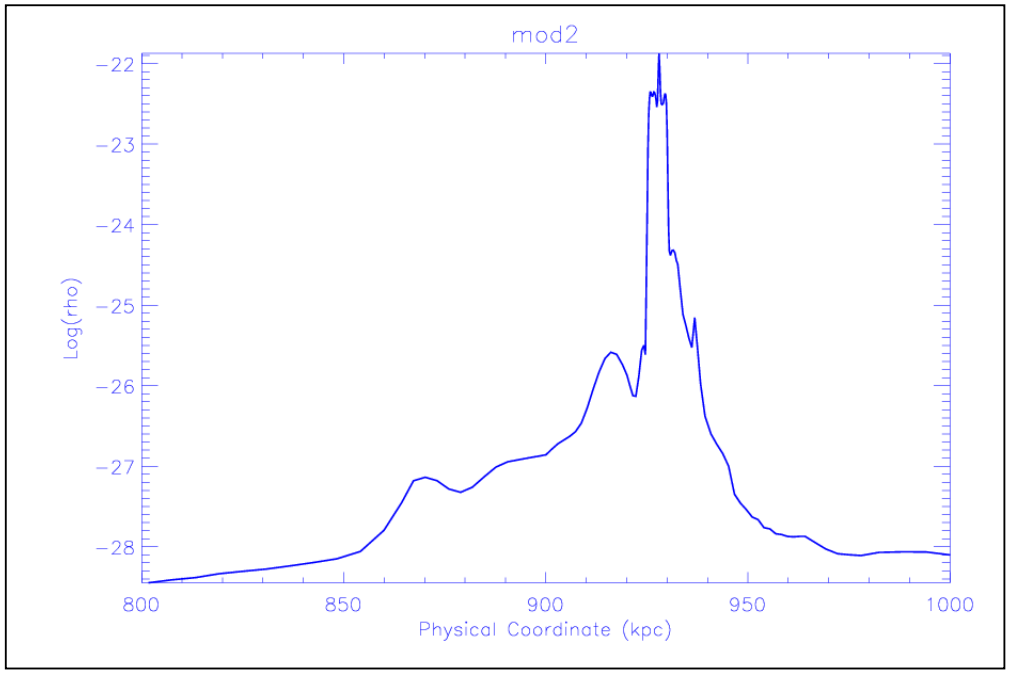

Figure 6.15 Total density (rho) vs. physical coordinate along z for mod2.

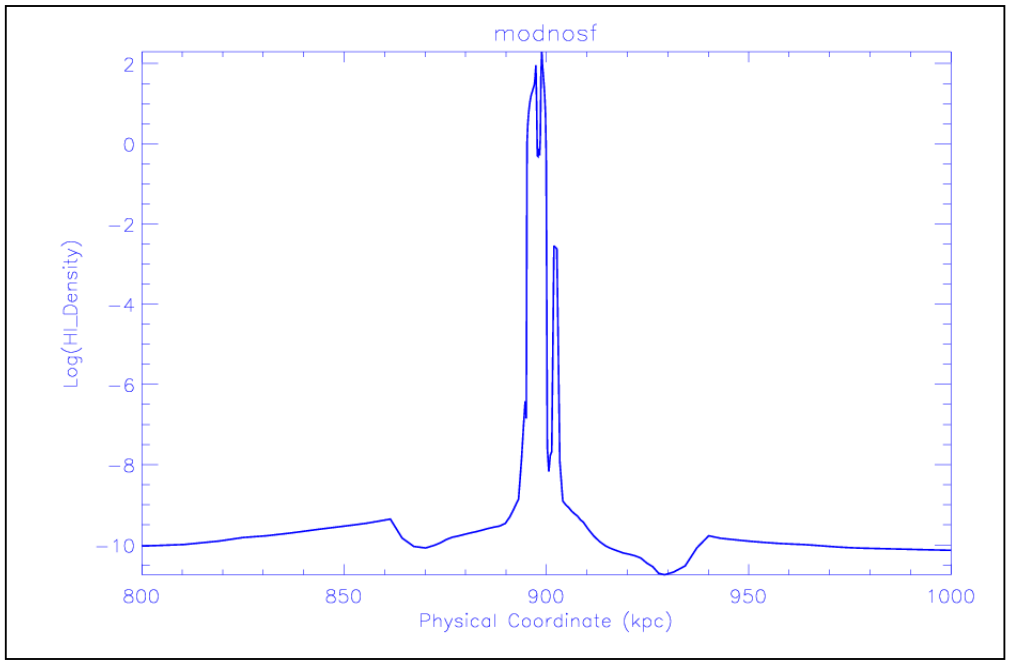

Figure 6.16 HI density vs. physical coordinate along z for modnosf.

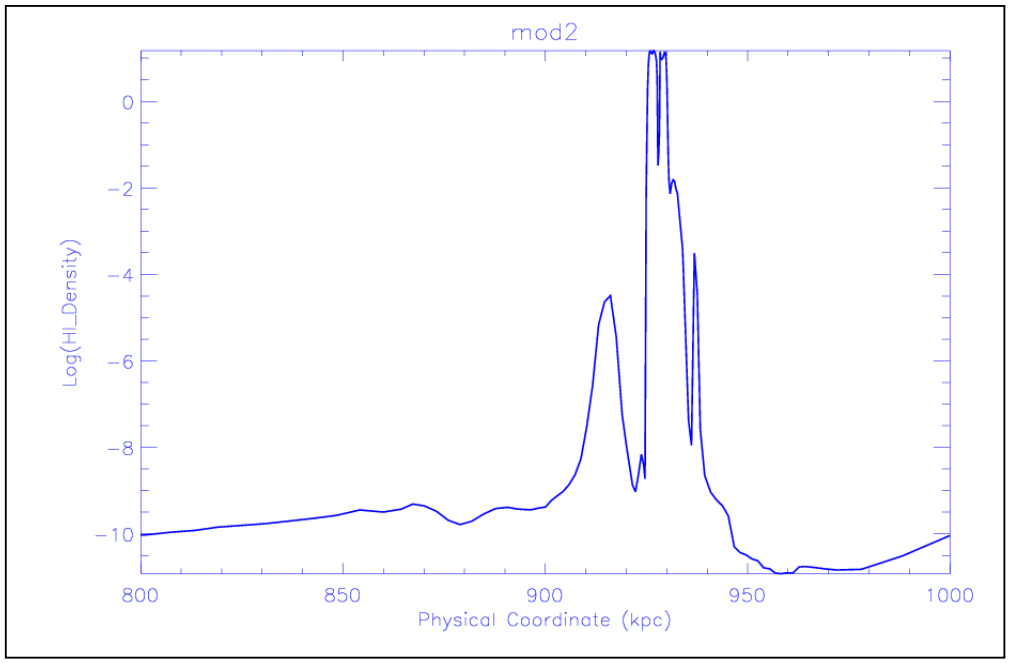

Figure 6.17 HI density vs. physical coordinate along z for mod2.

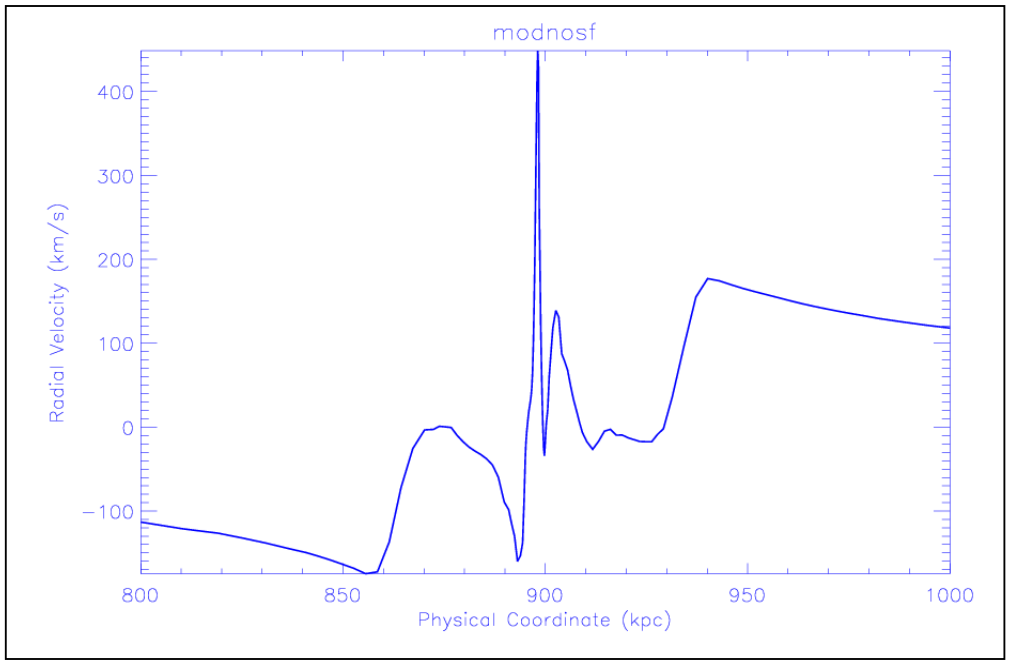

Figure 6.18 Radial velocity vs. physical coordinate along z for modnosf.

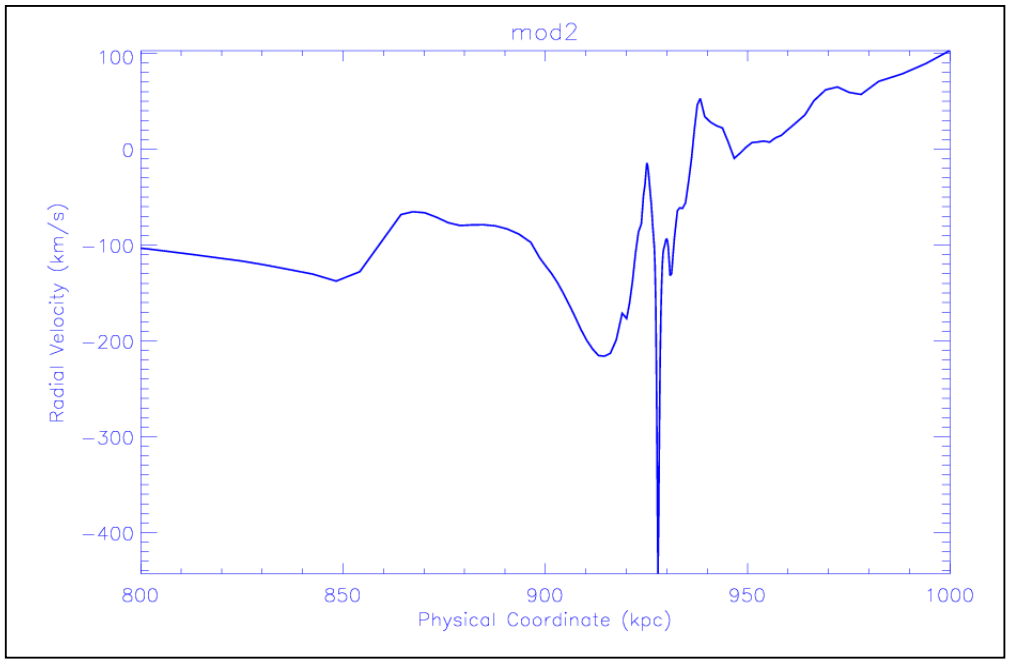

Figure 6.19 Radial velocity vs. physical coordinate along z for mod2.

6.5 Summary

We found that radiative transfer does play an important role in reproducing DLA abundance. Star formation and feedback do not have a large effect in general. This might be due to the low grid-resolution, small volume box size, and non-linearity of star formation effect. However, star formation/feedbacks do produce some local violent activities at regions with relatively high velocity dispersions. To summarize, it is essential to include radiative transfer into all runs. Although we are able to reproduce DLA column density distribution, we still have lower velocity widths than are observed. In the current stage of our research, star formation does not solve the low velocity width problem in our simulations since star formation effects are non-linear effect. For example, increased star formation/feedback might destroy neutral clouds that provide material for next generation star formation. Hence, low velocity width would be observed. We are not certain this type of event, however, would happen at which step. Therefore, further investigations are needed. We also need to cover the parameter space in more detail in order to find the precise star formation and feedback strength parameters input to produce the maximum effect.

6.6 Future Work

We plan to continue the research with improved computing technique and physics based on our previous work. Future simulations would include new physical ingredients, such as full radiative transfer with local and non-local UV backgrounds, large volume size for creating higher-mass cluster of galaxies, and higher grid resolution to resolve substructures in detail. Our first step is to explore the parameter space with the same 64^3 resolution and refinement level to seek the star formation/feedback parameters input that would give rise the best and maximum star formation effect. We will then apply this information to higher grid-resolution and larger volume size simulations. Finally, we would consider possible additional physical assumption, such as warm, dark matter cosmology.

References

References

Abel, T., Norman, M.L., & Madau, P. 1998, astro-ph/9812151

Gardner, J. P., Katz, N., Hernquist, L., & Weinberg, D. H. 1997, ApJ, 484, 31

Gardner, J. P., Katz, N., Hernquist, L., & Weinberg, D. H. 2001, ApJ, 559, 131

Haehnelt, M. G., Steinmetz, M., & Rauch, M. 1998, ApJ, 495, 647

Hu, E. M., Kim, T. S., Cowie, L. L., Songaila, A., & Rauch, M. 1995, astro-ph/9507047

Maller, A. H., Prochaska, J. X., Somerville, R. S., & Primack, J. R. 2001, MNRAS, 326, 1475

Mellema, Garrelt., Iliev, I. T., Alvarez, M. A., & Shapiro, P. R. 2005, astro-ph/0508416

Katz, N., Weinberg, D. H., Hernquist, L., & Miralda-Escude, J. 1996, ApJ, 457, L57

Nagamine, K., Springel, V., & Hernquist, L. 2004, MNRAS, 348, 435

Nagamine, K., Springel, V., & Hernquist, L. 2004, MNRAS, 348, 421

O'Shea, B. W. et al. 2004, astro-ph/0403044

Press, W. H. & Schechter, P. 1974, ApJ, 187, 425

Prochaska, J. X., Herbert-Fort, S., & Wolfe, A. M. 2005, astro-ph/0508361

Prochaska, J. X. & Wolfe, A. M. 1997, ApJ, 487, 73

Prochaska, J. X. & Wolfe, A. M. 2001, ApJ, 560, L33

Razoumov, A. O., Norman, M. L., Prochaska, J. X., & Wolfe, A. M. 2005, astro-ph/0510786

Sommer-Larsen, J., Götz, M., & Portinari, L. 2003, astro-ph/0204366

Springel, V. & Hernquist, L. 2002, MNRAS, 333, 649

Wolfe, A. M., Gawiser, E., & Prochaska, J. X. 2005, ARA&A, 43, 861

VITA

Yi-Jung Yang was born in Taitung, Taiwan ROC on March 12, 1976. After receiving a two-year degree in English from Taiwan Adventist College, she entered Kutztown University of Pennsylvania in the United State in 1998, and received a Bachelor Degree in Physics in May 2001. She entered The University of Tennessee, Knoxville in August 2001, and received a Master of Science Degree in physics in August 2006. Her research interests include Cosmology, Astrophysics, Plasma and Fusion Science, and High Energy Physics.